

## Review

Subrata Batabyal, Susobhan Choudhury, Dilip Sao, Tanumoy Mondol and Samir Kumar Pal\*

# Dynamical perspective of protein-DNA interaction

**Abstract:** The interactions between protein-DNA are essential for various biological activities. In this review, we provide an overview of protein-DNA interactions that emphasizes the importance of dynamical aspects. We divide protein-DNA interactions into two categories: non-specific and specific and both the categories would be discussed highlighting some of our relevant work. In the case of nonspecific protein-DNA interaction, solvation studies (picosecond and femtosecond-resolved) explore the role environmental dynamics and change in the micropolarity around DNA molecules upon complexation with histone protein (H1). While exploring the specific protein-DNA interaction at  $\lambda$ -repressor-operator sites interaction, particularly  $O_{R1}$  and  $O_{R2}$ , it was observed that the interfacial water dynamics is minimally perturbed upon interaction with DNA, suggesting the labile interface in the protein-DNA complex. Förster resonance energy transfer (FRET) study revealed that the structure of the protein is more compact in repressor- $O_{R2}$  complex than in the repressor- $O_{R1}$  complex. Fluorescence anisotropy studies indicated enhanced flexibility of the C-terminal domain of the repressor at fast timescales after complex formation with  $O_{R1}$ . The enhanced flexibility and different conformation of the C-terminal domain of the repressor upon complexation with  $O_{R1}$  DNA compared to  $O_{R2}$  DNA were found to have pronounced effect on the rate of photoinduced electron transfer.

**Keywords:** different dynamical conformations; molecular recognition; operator DNA; photoinduced electron transfer; protein-DNA interactions; protein-DNA interface; resonance energy transfer; solvation dynamics.

\*Corresponding author: Samir Kumar Pal, Department of Chemical, Biological and Macromolecular Sciences, S. N. Bose National Centre for Basic Sciences, Block JD, Sector III, Salt Lake, Kolkata 700 098, India, e-mail: skpal@bose.res.in

Subrata Batabyal, Susobhan Choudhury, Dilip Sao and Tanumoy Mondol: Department of Chemical, Biological and Macromolecular Sciences, S. N. Bose National Centre for Basic Sciences, Block JD, Sector III, Salt Lake, Kolkata 700 098, India

## Introduction

Protein and DNA are two of the most important biomolecules in any living organism (1–5). DNA stores the genetic information, while protein takes care of executing and regulating the life processes. Protein-DNA interactions therefore play a crucial role in central biological processes, ranging from the mechanism of replication, transcription and recombination to enzymatic events utilizing nucleic acids as substrates (6–8).

Protein-DNA interaction can be broadly classified into two types – nonspecific and specific interaction (9). Structural proteins that bind DNA are well-understood examples of nonspecific DNA-protein interactions. From a mechanistic standpoint, the non-sequence-specific interaction between nucleic acids and proteins can be qualitatively understood on the basis of relatively simple physicochemical principle. Histone (protein)-DNA interactions are an example of such interactions, and they occur between functional groups on the protein and the sugar-phosphate backbone of DNA. In the case of nonspecific interactions, the sequence of nucleotides does not matter, as far as the binding interactions are concerned. Through nonspecific interaction, structural proteins help to organize DNA into compact ‘chromatin’ form (Figure 1). Specific DNA-protein interactions, however, depend upon the sequence of bases in the DNA. Specific protein-DNA interaction (9) is governed by sequence recognition (base readout) through direct contacts between protein’s amino acid side chains and DNA bases (10), as well as the spatial geometry of the two biomolecules (shape readout) (10). Recognition of specific DNA sequences by specific DNA-binding proteins often leads to the formation of large protein complexes responsible for regulation of gene expression. Biological function of the protein-DNA conjugates often depend on the conformational dynamics, local solvation, and micropolarity after complexation. In a variety of biological processes, the conformational flexibility of the protein upon DNA binding is the key signal for the further propagation of the process. The molecular bases of the remarkably accurate recognition of particular nucleotide sequences by site-specific proteins comprise one of the major

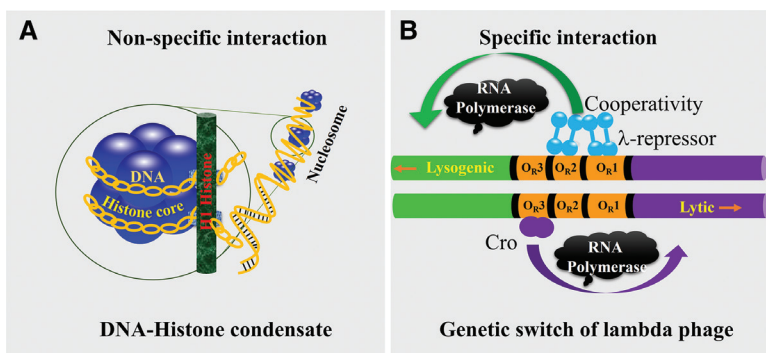


**Figure 1** Schematic representation of non-specific (DNA-histone I) and specific protein-DNA (operator DNA with lambda/corepressor) interaction and their implications.

unsolved puzzles of present day molecular biology. A long-standing but yet unattained objective in structural biology is to elucidate the physicochemical basis of the specific and nonspecific interaction between various protein-protein and protein-DNA (biomolecular recognition), leading to the regulation of gene expression. In this regard, dynamics of biomolecular recognition is of crucial importance. Many factors may contribute in this process of complex recognition process. Recent works on specific and nonspecific protein-DNA interactions have demonstrated effects of binding rigidity, local solvation and micropolarity on the biological function of the complexes (11–17). In the recent past, there has been some advancement in the exploration of the dynamical perspective of protein-DNA interaction. An interesting series of works have been published by Kalodimos et al. on the binding of DNA to several variants of the catabolite activator protein (CAP), which differentially populate the inactive and active DNA-binding domain states (18, 19). The allosteric control of the CAP protein has been comprehensively elaborated in several of their recent publications (20) and interested readers are highly encouraged to go through the original publications.

DNA-protein interactions are studied using a variety of methods such as gel-shift assays, foot-printing, NMR structural studies (21), X-ray crystallographic studies (21) and fluorescence spectroscopy. Among all the possible methodologies, fluorescence polarization/anisotropy provides a rapid, non-radioactive method for accurately measuring DNA-protein interaction directly in solution. In this review, we provide a revised view of protein-DNA interactions that emphasizes the importance of the dynamical aspects and conformational changes of both macromolecules. The experimental techniques are mainly based on fluorescence spectroscopy. In order to reassess protein-DNA interaction, we have divided this review into two main sections. For the nonspecific protein-DNA

interaction, the interaction of histone protein with DNA is elaborated in great detail (17, 22). The studies of the nature of binding interactions and dynamics of protein histone I (H1) with ligands in solution and as a complex with DNA, an important biological process for the higher-order structure in chromatin are discussed. While elaborating the important aspects of specific protein-DNA interaction, the complexation of lambda repressor protein with different operators is explored (Figure 1).

Structurally  $\lambda$ -repressor is a two domain protein. The N-terminal domain interacts with the DNA (16), while the C-terminal domain is responsible for most protein-protein interactions (23); these interactions are essential for the co-operative binding (24, 25) and for the functioning of the genetic switch (11, 26).

## Methodology

In this review, the experimentally obtained results are the outcome of the various fluorescence spectroscopic tool and analytical methods. Steady-state absorption and emission spectrophotometers were used to measure the sample concentration and steady-state fluorescence emission. More sophisticated time-resolved fluorescence techniques were used to monitor dynamical aspects in the femtosecond to picosecond time domain (17, 22). Details of the time-resolved techniques are available in the published literature (27, 28). In order to explore biomolecular recognition, microfluidics approach coupled to fluorescence microscopy was employed (27, 29). The most useful technique, often termed as the molecular ruler, FRET (30, 31), was used to monitor the distance between donor and acceptor molecules. Furthermore solvation analysis of the excited fluorophore was used to envisage the immediate environments and hence to detect the effect of the interaction of protein-DNA (31).

## Results and discussion

### Nonspecific protein-DNA interaction

In this section we have highlighted the structural and dynamical aspects of DNAs from various sources including synthetic oligonucleotides and as a complex with histone1 (H1) in the nonspecific protein-DNA interaction.

#### Picosecond-resolved dynamics at the protein-DNA interface: histone-DNA complexes in aqueous solution (22)

Genomic DNAs extracted from calf functional thymus and salmon testes are known to form complexes with the linker histone H1 through a nonspecific interaction. The schematic representation of the complexes is shown in Figure 1. Though both calf thymus and salmon sperm DNA interact with H1, the ultimate structure of the complexes differs substantially. TEM study reveals the compact nature of the calf thymus DNA-H1 complex (DNA and protein are from the same species; intra-species) compared to that of the salmon sperm DNA-H1 (interspecies) and were found to be caused by the greater compactness of intra-species DNA condensates than that of the interspecies DNA condensates.

In order to provide detailed dynamical aspects of such protein-DNA condensates, minor groove binder dye Hoechst 33258 (H33258) was used. Figure 2(A) shows the emission spectra of the probe H33258 in the calf thymus DNA and DNA-H1 complex. In hydrophobic environments the dye shows blue shift (32). The emission maxima of the ligand in buffer and in DNA are 515 and 470 nm, respectively. The ligand bound to the DNA-H1 complex shows an emission maximum at 460 nm, indicating more non-polar environments of the probe in the DNA upon complexation with H1. The fluorescence transients of H33258-calf thymus DNA in buffer at three characteristic wavelengths are shown in Figure 2(B). The numerical fittings (solid lines) of the data are made up to 35 ns. The change in the transient in the blue side of the emission spectra from that in the red side, are shown in the 6 ns time window. The transients with a systematic series of wavelength detection from 410 to 600 nm with a 10 nm regular wavelength interval show three distinct time scales of ~150 ps, ~2.2 ns, and ~4 ns. The blue wavelength (410 nm) decays with 150 ps time constant and rises with a similar time constant at the red side (600 nm), which is the signature of solvation dynamics (33). Other two time constants remain similar

in all of the wavelengths of detection. The time-resolved emission spectra (TRES) of the H33258-calf thymus DNA complex up to 15 ns is shown in Figure 2(C). The net spectral shift is 1715/cm (from 21 514 to 19 799/cm in 35 ns). It should be noted that the emission peak of H33258 in non-polar dioxane is 22 935/cm (34). The difference of the peak value of H33258 in DNA environments at  $t=0$  from that of the peak in the non-polar medium reflects the missing dynamics of the corresponding environments within the instrumental resolution (35). Figure 2(D) demonstrates that the time evolution of the spectral peak frequency of H33258 attached to calf thymus DNA and in the DNA-H1 complex. The data points are fitted with a biexponential decay function yielding different solvent relaxation time constants for the DNA in different environments. The dynamics of the H33258-calf thymus DNA complex shows two distinct time constants of 250 ps and 13.50 ns.

The time scales obtained from our experiment are similar to the relaxation times seen in the coumarin-modified DNA (36). The time constants are much slower than the low-frequency vibrational motion of DNA or quasi-harmonic oscillation of a fluorophore within a static DNA structure and are close to the diffusive reorganization of a liquid (36). The faster time constant of 250 ps may be caused by the relaxation of the DNA structure. The longer time constant (13.50 ns) arises from the diffusive motion. As evidenced in Figure 2(E), H33258 in salmon sperm DNA shows two dynamical time constants of 70 ps and 13.60 ns. The dynamical time constants of H33258 in DNA-H1 are 60 ps and 10.44 ns, which are similar to that of the DNA without H1. The solvation features in the different environments are similar to that in the respective environments of the calf thymus DNA. Structural X-ray crystallographic and NMR studies (37) on the ligand with duplex1 show that the specific sequence of (CGCAAATTTGCG) of the DNA is extremely important for the ligand H33258 binding. Solvation dynamics study (Figure 2F) of the ligand bound oligonucleotide reveals two time constants of 60 ps and 8.50 ns. In the duplex1-H1 complex, the time constants change to 120 ps and 25 ns. The observation of slower relaxation dynamics of the probe in the duplex1-H1 complex is not consistent with those in the genomic DNAs. The poly GC sequence of duplex2 (GCGCGCGCGCGC)<sub>2</sub> is ideal for the intercalative mode of EtBr-binding (38). The significant change in the fluorescence intensity and lifetime of the probe EtBr upon binding to DNA and DNA-H1 complex is used to explore the perturbation of intercalative interaction of the ligand in the DNA condensate.

The significant decrease in emission intensity and shift toward the red wavelength (622 nm) of EtBr in the DNA-H1 complex compared to EtBr-DNA in the bulk buffer

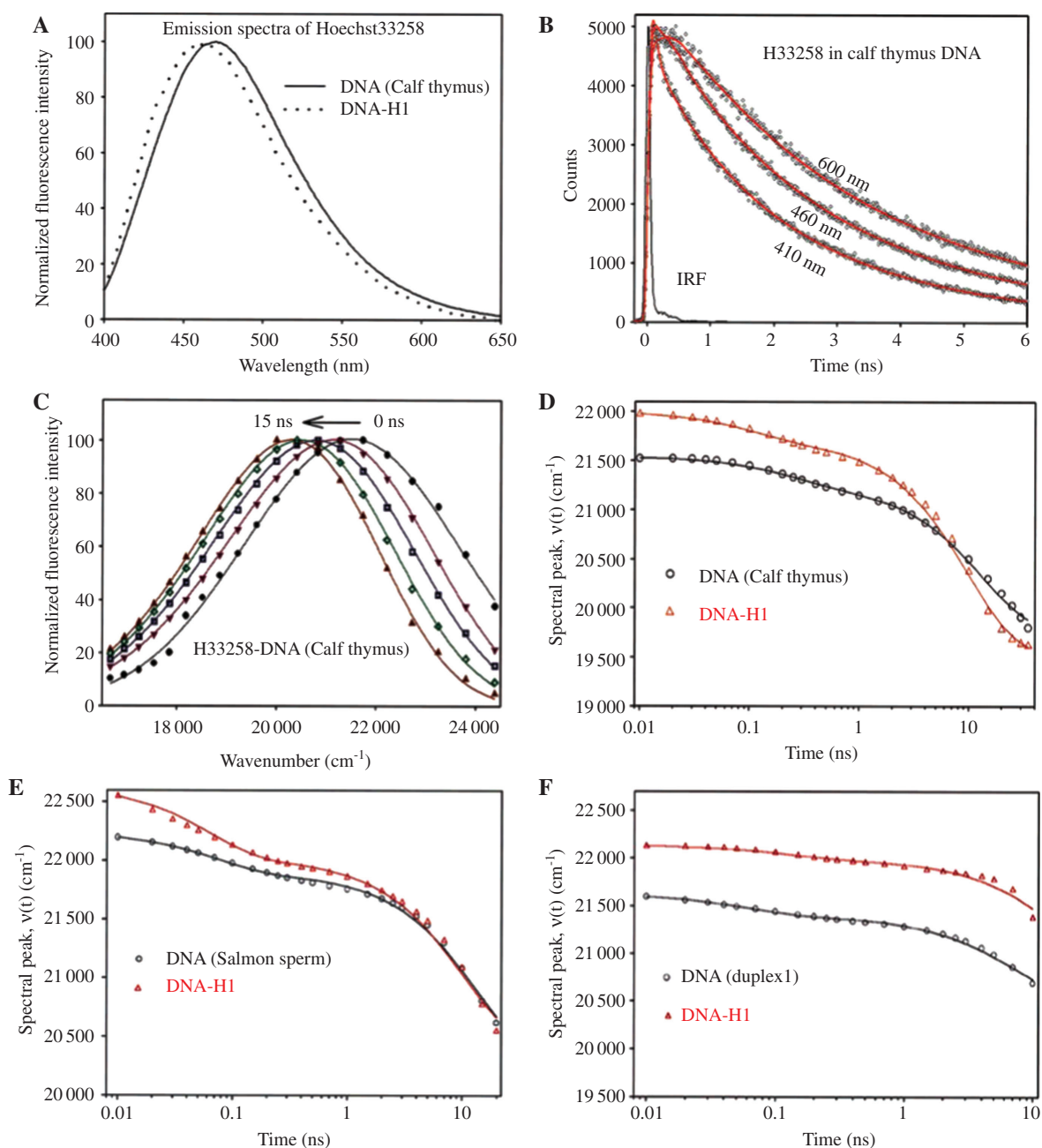


**Figure 2** Solvation relaxation of H33258 in DNA and in DNA-Histone complex.

(A) Steady-state emission spectra of H33258 in calf thymus DNA and the DNA-H1 complex. (B) Fluorescence transients of H33258-calf thymus DNA at three different detection wavelengths. (C) Time-resolved emission spectra of H33258 in calf thymus DNA. Time-resolved fluorescence spectral peak frequency of H33258 in (D) calf thymus DNA and DNA-H1 complex, (E) salmon sperm DNA and its condensate, and (F) duplex1 and duplex1-H1 complex are shown. Solid lines indicate biexponential numerical fitting of the experimental data points. [Reprinted with permission from ref. (22) Copyright 2007, American Chemical Society.]

as evidenced from Figure 3(A) is indicative of the reduction of binding strength of EtBr-binding to the DNA upon complexation with H1. The observations find similarity with other reports in the literature (39). Picosecond-resolved transients of EtBr-calf thymus DNA complexes are shown in Figure 3(B). As shown in Figure 3(B) the

maximum population [22 ns (73%)] of the dye is intercalated to the DNA. The transient of EtBr in the DNA-H1 complex shows that the contribution of a longer ~22 ns (2%) decay component decreases considerably, reflecting significant decrease in the binding affinity of EtBr in the DNA condensate. The binding constants of EtBr in

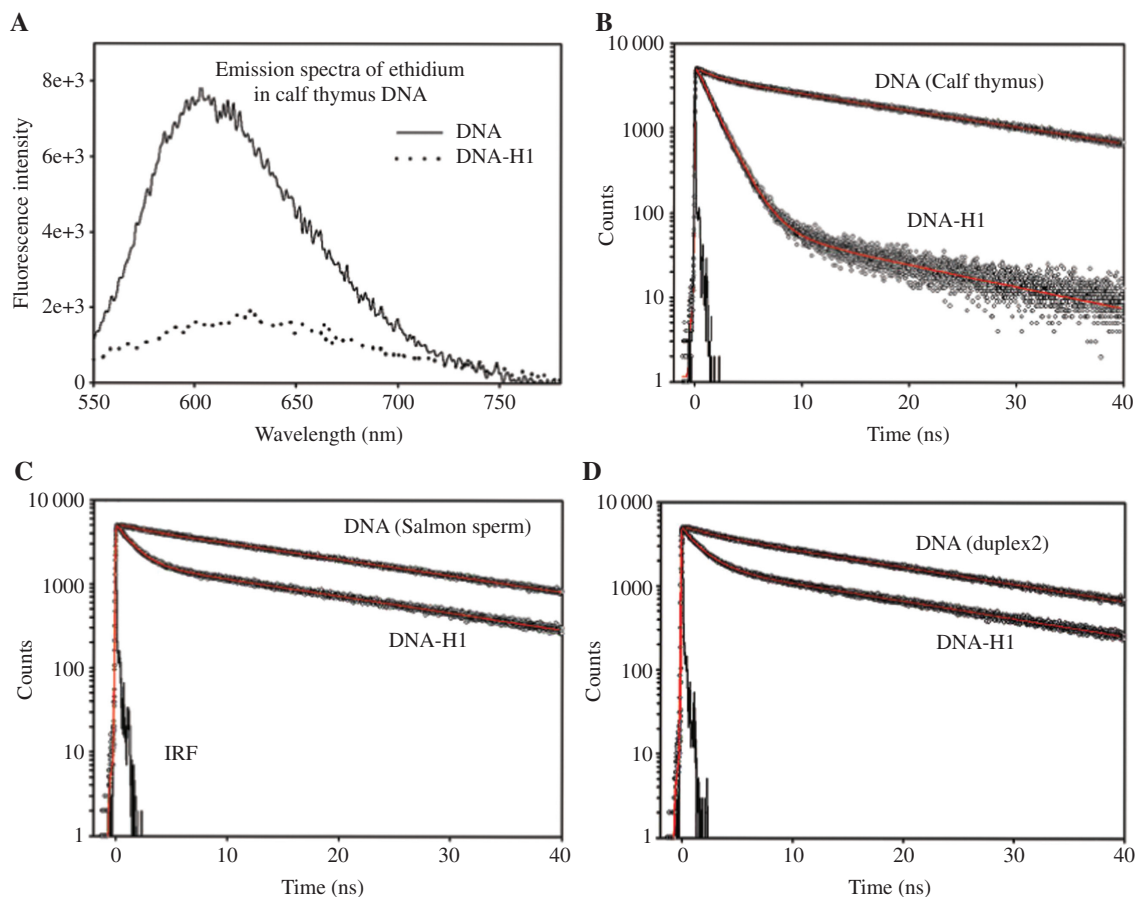


**Figure 3** FRET study in DNA-Histone I complex.

(A) Steady-state emission spectra of EtBr in calf thymus DNA and DNA-H1 complex are shown. Picosecond-resolved fluorescence transients of EtBr in (B) calf thymus DNA, (C) salmon sperm DNA, and (D) duplex2 and their condensates are shown. Solid lines indicate biexponential numerical fitting of the experimental data points. [Reprinted with permission from ref. (22) Copyright 2007, American Chemical Society.]

the DNA and DNA-H1 complex are shown in Table 1. In order to investigate the ligand binding of the interspecies DNA-H1 complex, the complexation of EtBr-salmon sperm DNA with calf thymus H1 was investigated. The decrease in fluorescence intensity (data not shown) and change of the contribution of a longer [22 ns (34%)] time constant of the EtBr-DNA-H1 complex [Figure 3(C) and Table 1] are less than that of the calf thymus DNA condensate. The observation is consistent with the fact that the intercalative interaction of EtBr with the salmon sperm DNA condensate is much stronger than that with the calf thymus DNA condensate. The stronger interaction in the salmon sperm DNA condensate is correlated with the less-compact structure of the DNA-H1 complex as evidenced from TEM experiments. In order to study the effect of a base pair sequence in the molecular recognition of the DNA-H1 complex, oligonucleotide sequence of duplex2 was deliberately chosen. EtBr strongly intercalates to GC enriched homo oligonucleotides. From Figure 3(D) and Table 1, it is

evident that the perturbation of EtBr-binding (change in 22 ns component) to the duplex2 upon complexation with H1 is less compared to both calf thymus and salmon sperm DNA condensates. From Table 1, it is evident that the faster time constant (<3.5 ns) of EtBr in the duplex2 without H1 is slower than that in buffer (1.5 ns) and much faster than

**Table 1** Picosecond-resolved fluorescence transients of ethidium in various DNAs and their condensates with H1.

| DNA type         | System | Binding constant (M <sup>-1</sup> ) | $\tau_1$ (ns) with % | $\tau_2$ (ns) with % |
|------------------|--------|-------------------------------------|----------------------|----------------------|
| Calf thymus DNA  | DNA    | $5.30 \times 10^4$                  | 1.46 (27%)           | 22.36 (73%)          |
|                  | DNA-H1 | $4.08 \times 10^2$                  | 1.52 (98%)           | 15.34 (2%)           |
| Salmon sperm DNA | DNA    | $1.51 \times 10^5$                  | 1.14 (12%)           | 22.45 (88%)          |
|                  | DNA-H1 | $1.08 \times 10^4$                  | 1.49 (66%)           | 21.70 (34%)          |
| Duplex2          | DNA    | $7.74 \times 10^4$                  | 3.51 (15%)           | 21.42 (85%)          |
|                  | DNA-H1 | $3.45 \times 10^3$                  | 1.85 (65%)           | 20.83 (35%)          |

that of the DNA-bound EtBr through intercalative interaction (22 ns). The time constant may indicate that EtBr molecules are loosely bound to the DNA through non-intercalative interaction, namely electrostatic binding (40). However, in the duplex2-H1 complex, the loosely bound EtBr molecules are detached and show a time constant of 1.8 ns similar to that in the bulk buffer (1.5 ns).

The discussed studies on various kinds of DNA molecules in solution and upon complexation with H1, show the nature of change of the local environments of the DNA molecules in the complex. In the case of genomic DNA molecules, the solvation studies depict an insignificant change in the local environments of DNA molecules upon complexation with H1. Fluorescence anisotropy studies on the minor groove binder H33258 in DNA and in the complex clearly rule out the possibility of detachment of any minor groove-binding drug with the DNA in the complex (data not shown). In contrast to the minor groove-binding, a significant perturbation in the intercalative interaction of EtBr with various DNA molecules including synthetic oligonucleotide upon complexation with H1 clearly demonstrate that the base-stacking is heavily perturbed in the DNA-H1 complexes. Circular dichroism (CD) studies reveal significant alteration in the conformation of genomic DNA molecules upon complexation with H1, which is consistent with the condensed C form (data not shown). Perturbation of base-stacking as revealed by intercalation of EtBr could be the consequence of the change in the conformation of the DNA in the complex. These observations are important to understand the binding of drug molecules in the linker DNA of nucleosome core particles.

### Femtosecond resolved solvation and charge transfer dynamics at histone I-DNA interface (17)

In another study, Zewail et al. explored the nature of binding interactions and dynamics of protein histone I (H1) with ligands in solution and as a complex with DNA in femtosecond time resolution (17). Both covalent and noncovalent labeling on the protein was carried out using 2-(p-toluidino)naphthalene-6-sulfonate (TNS) and 5-(dimethylamino)naphthalene-1-sulfonyl chloride (DC), respectively. The study aimed to unravel the solvation dynamics, which occur within 1 ps, for the probe at the protein surface and in bulk solution, and hence exploring the role of biological water in protein-DNA interaction. We will briefly discuss the important finding of the study and its relevance in biological aspects.

Upon the addition of protein histone (H1) to an aqueous solution of TNS the fluorescence emission increases by 60

times and the ‘maximum’ shifts to the blue by 40 nm, from 470 nm in pure water to 430 nm (325 nm excitation); see Figure 4(A). The formation of H1-DNA complexes (deoxyribonucleic protein, DNP) results in an 11-fold decrease in fluorescence, compared to that of H1 alone. When DC is covalently attached to H1 (DC-H1 adduct), compared to DC in MeOH at the same optical density, the fluorescence emission increases by about a factor of 2. The spectrum is 25 nm blue shifted. However, the fluorescence intensity and profile remain unchanged when the adduct forms a complex with DNA, as shown in Figure 4(B).

The transients of TNS in H1 solutions are shown in Figure 5 for three typical wavelengths (the blue edge,

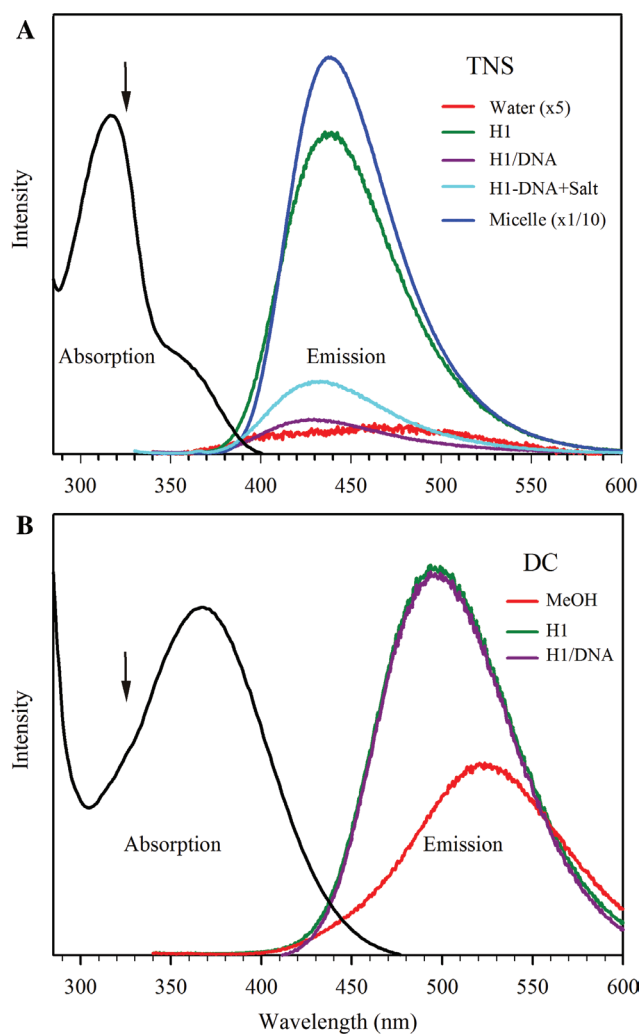


**Figure 4** The steady-state fluorescence spectra of the probes (A) TNS and (B) DC in chemical and biological environments studied with the same probe concentration. The absorption spectra are also shown and the arrows mark the excitation wavelength (325 nm). Note the huge enhancement in emission of TNS in H1 and the micelle. [Reprinted with permission from ref. (17) Copyright 2001, Wiley-VCH-Verlag GmbH.]

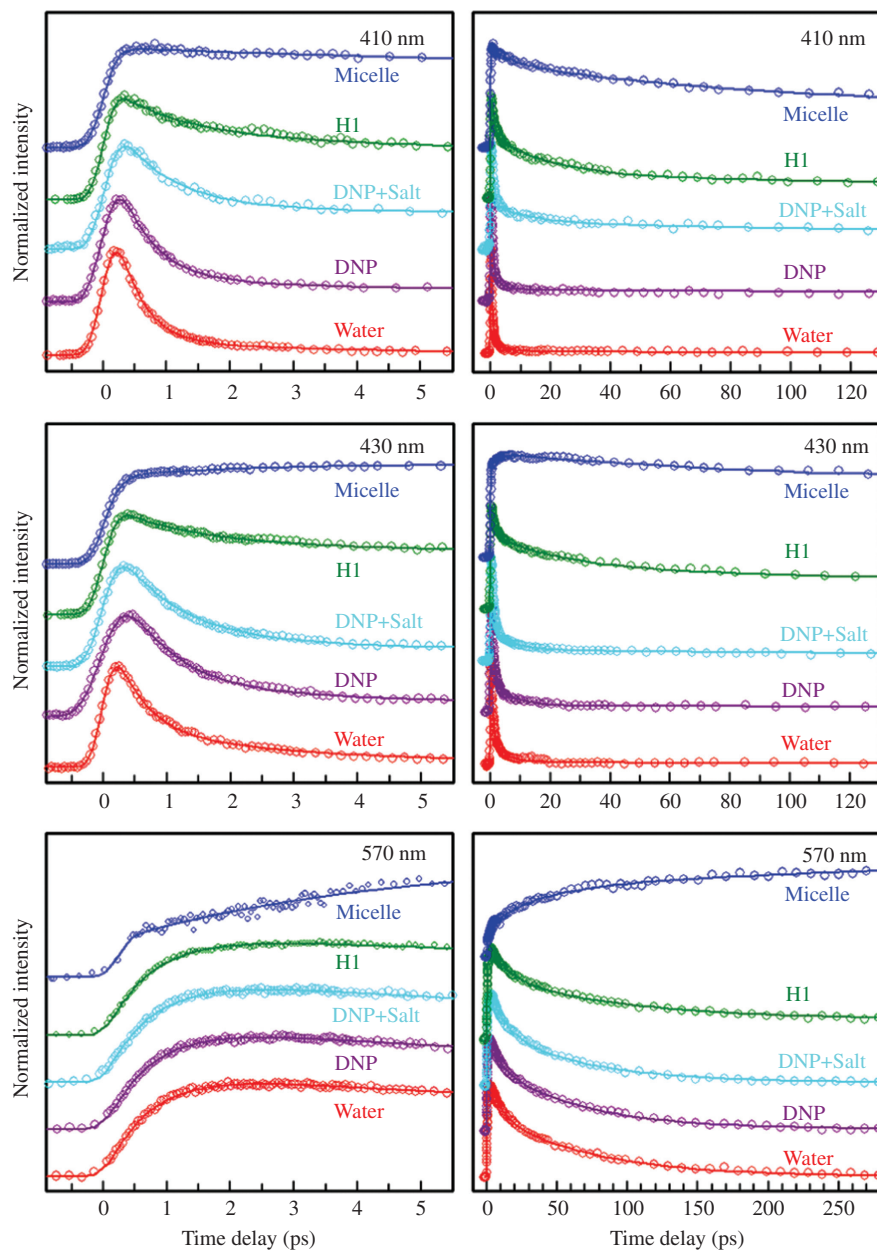


**Figure 5** The observed transients of TNS in water, the different biological environments studied, and in cationic micelles.

Two time scales are shown, short (left) and long (right), for three typical fluorescent wavelengths: the blue side, emission peak, and the red side. Note the change in time scale for the 570 nm case at long times. All transients are normalized for comparison. [Reprinted with permission from ref. (17) Copyright 2001, Wiley-VCH-Verlag GmbH.]

peak, and red-tail emission). This result is surprising given that the common picture for protein solvation is one in which the protein involves a water layer that is different from bulk water. However, if solvation is dominated by long range water shells or involves networks of water structures then the  $\sim 700$  fs solvation time characteristic of bulk water is not surprising. Using the surface-sensitive second harmonic generation detection, the observation indicates that the rigid structure of water molecules on the surface of the random-coiled termini does not play a

significant role. Solvation in such rigid structures gives rise to dynamics on slower time scales and has recently been reported (41, 42). The protein water 'layer' is dominant in the hydrophobic globular domain and is used effectively to conserve the folded structures. The probe ligand interacts with the N and C termini by electrostatic interactions. The addition of DNA to H1-TNS complexes displaces the TNS molecules (Figure 4), and it is known that DNA binds to H1 mainly through N and C termini (43). The evidence of the TNS-hydrophobic interaction picture stems from the

comparison of the steady-state emission in polar and non-polar solvents, with the latter being similar in peak position to that in protein solution. The micropolarity near the interface between the ligand and the protein is determined by the combined dielectric constants of the two components (44). In fact, the emission peak in protein solution is at 430 nm whereas in the less-polar solvent (THF) it is at 420 nm. The micropolarity was probed by the twisting motion of the ligand, which takes longer in proteins than in water: 3.5 (410 nm), 9 (430 nm, emission peak), 10.5 (470 nm), 14 (510 nm), and 15 ps (570 nm). This lengthening reflects the increase in the effective twisting barrier in the protein environment. The long time components (100 ps or longer) are greatly enhanced, consistent with a substantial trapping of molecules in the locally excited (LE) state (following solvation) because of the increase in barrier height. The observed huge enhancement of the steady-state fluorescence emission (Figure 4A), therefore, results from the trapping of the molecules in the LE state (Figure 6A). The charge transfer (CT) state near the protein site must increase its energy in order for this trapping to

be efficient; CT non-radiative decay also decreases as the CT shifts to higher energy. Accordingly, the effective dielectric constant must be smaller than that of bulk water. At an interface, the ligand molecule experiences the polarity from both sides (44) and the net local polarity is lower than that of the bulk. The increase in the barrier energy is dominated by the polarity effect (higher CT energy). This is evidenced by the similarity in time scales for the fraction of the molecules that undergo twisting above the barrier (25%, 10 ps). The restriction on the twisting motion of TNS by the protein H1 is not significant because TNS interacts interfacially and is not housed in the rigid protein pocket. This is further supported by measurements of the local motion of the ligand (anisotropy studies). In the micelle, no twisting motion was observed and all molecules are trapped in the LE state. The lifetimes increase to tens of nanoseconds, and emission becomes 670 times stronger. These results indicate that charge separation and twisting motion do not occur in the excited state because of the lower dielectric constant and the high microviscosity in the layer of the micelle. To probe the local rigidity of ligand-protein complex, we measured the time-resolved anisotropy of TNS at the peak emission of 430 nm, shown in Figure 7A. It has three decay components: the major contribution (~75%) of the anisotropy decays with ~75 ps time constant and the final anisotropy is close to zero (0.015); the initial drop of the minor contribution occurs on the time scale of solvation and twisting. Because of its similarity to other anisotropy decays, the ~75 ps decay represents the diffusive motion of TNS at the terminal surface. Apparently, the electrostatic attraction does not place a significant restriction on the orientational motion of TNS, again consistent with the idea that it is not in a complete rigid layer. The picture envisaged is that the TNS molecule is labile on the H1 surface with the negative charge pointing to the cationic termini. In contrast, the anisotropy of TNS in the micelle is persistent, as shown in Figure (7A). It has a single exponential decay of ~800 ps, a long orientation relaxation process. This significant increase in the relaxation time is caused by the large rigidity in the Stern layer. The fact that the anisotropy did not decay to zero, up to 500 ps, elucidates the rigidity of the entire molecule toward rotations. The lack of a 2 ps decay is consistent with the hindrance of the intramolecular twisting motion; only the slow solvation dynamics in the LE state proceeds.

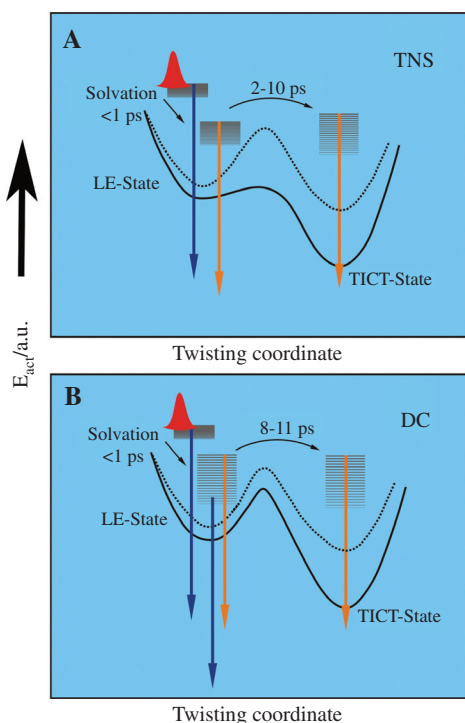


**Figure 6** Schematic potential energy curves along the reaction coordinate (twisting) for the two probes (A) TNS and (B) DC with the observed emission.

The dashed lines present the potential energy curves when the probe binds to the protein H1. The barriers are increased mainly because of the lower micropolarity on binding sites. Note the nearly barrier-less twisting motion for TNS in pure water. [Reprinted with permission from ref. (17) Copyright 2001, Wiley-VCH-Verlag GmbH.]

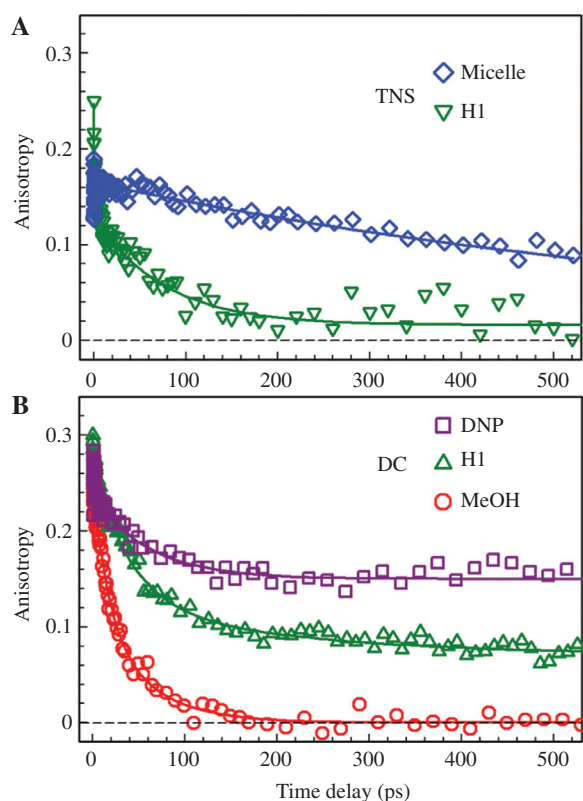


**Figure 7** Femtosecond-resolved fluorescence anisotropy in different environments for (A) TNS (micelle, H1) and (B) DC (and DNP, H1, MeOH) at the peak emission.

Note the dramatic change for DC on going from free solvent MeOH to the protein H1 and to DNP. [Reprinted with permission from ref. (17) Copyright 2001, Wiley-VCH-Verlag GmbH.]

solvation dynamics on going from bulk to protein solutions, as also in the case of TNS/H1 system. This result is convincing because neutral DC is covalently connected to the protein binding sites. Similar to TNS in H1 solution, the twisting motion takes a longer time: 16 ps at 430 nm and 48 ps at 490 nm, which is caused by the increase of the twisting barrier. The fluorescence emission was blue shifted by  $\sim 20$  nm and the quantum yield increases by a factor of 2. These results again reveal the lower micropolarity at the interface of protein termini and water. The increase in quantum yield for DC is not as large as for TNS because of the trapping of DC molecules in the LE state (Figure 6B) and its large quantum yield (0.4) in bulk solvents. The anisotropy of DC is shown in Figure 7(B), together with that of DC in free MeOH for a comparison. In MeOH, the two major decay components have time constants of 14 (40%) and 50 ps (50%), except for a small initial decay ( $\sim 10\%$ ), which corresponds to the structure relaxation from ultrafast solvation. The 14 ps decay is similarly caused by the twisting motion. The time constant and percentage contribution are in good agreement with those observed at the magic

angle. The second component (50 ps) represents the orientation relaxation of DC. When DC is covalently connected to H1, the measured anisotropy dramatically changes and the time constants of the two major decay components increase to 40 and 207 ps. The anisotropy does not decay to zero, up to 500 ps. Both the twisting motion and the orientation relaxation slow down by a factor of about 4. The increase of the orientation relaxation time is caused by the covalent anchoring of DC to the H1 surface, which restricts the motion by the H1 backbone. The anisotropy due to the orientation relaxation (207 ps) decreases from 0.13 to the final value of 0.07. This change corresponds to an orientational motion in a cone with an estimated angle of  $\sim 20^\circ$ , reflecting a very restricted local motion. The whole DC-H1 complex relaxes on a much longer time scale. After complexation of TNS/H1 with DNA to form DNP, the fluorescence emission decreases considerably, by a factor of  $\sim 11$  (Figure 4A). The transients are shown in Figure 5 and are similar to those observed in bulk water. Because DNA and the TNS mainly bind to C and N termini of H1, the results indicate that DNA repels TNS out of the binding sites into the water solution. Thus, the ‘surface-surface’ electrostatic interaction between DNA and the protein H1 is much stronger than the ‘point-surface’ contact of TNS with H1. A small percentage of a long-time decay ( $\sim 500$  ps) component was observed for all wavelengths (Figure 5). In addition, the fluorescence profile is similar to that of TNS in the protein H1 (Figure 4A). Thus, this small fraction of TNS molecules ( $\sim 10\%$ ) left on the H1 surface probably reflects the hydrophobic binding interaction of TNS with the globular domain of H1.

Studies of femtosecond dynamics of ligand probes (TNS and DC) with the protein histone I and its DNA complexes elucidate the nature of the recognition process and the key time scales involved for complex rigidity, solvation, and micropolarity (Figure 9). These studies attempt to link structural and dynamical features for insight into the biological function of nucleosome formation and chromatin condensation. The rigidity of the protein-DNA complex was measured using the time-resolved anisotropy, which probes orientational motions of the ligand DC covalently adducted to the binding sites of the protein histone I. The anisotropy persists for more than 500 ps, in contrast to the behavior in the absence of DNA (200 ps) or in liquid methanol (50 ps). These results indicate the suppression of ligand motion in the complex; without DNA binding, the ligand experiences a motion in a cone with an angle of  $20^\circ$ . This relatively strong binding is also evident in the studies we made for the other ligand, TNS, which binds non-covalently to the protein. With DNA, the ligand is displaced (90%) elucidating the stronger

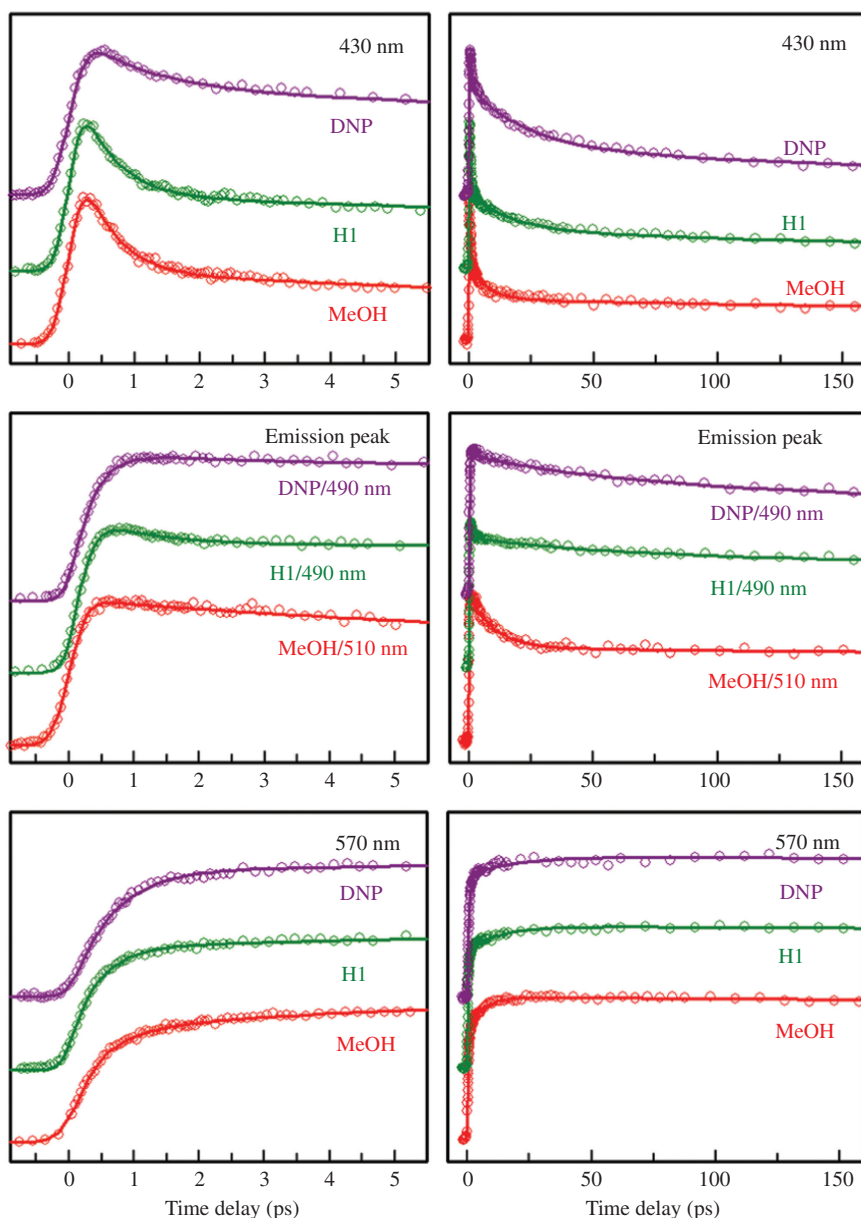


**Figure 8** The observed transients of DC in MeOH and the different biological environments studied.

Two time scales are shown, short (left) and long (right), for three typical fluorescent wavelengths: the blue side, emission peak, and the red side. Note the difference of transients for H1 and DNP, even though both have the same fluorescence emission (Figure 2B). All transients are normalized for comparison. [Reprinted with permission from ref. (17) Copyright 2001, Wiley-VCH-Verlag GmbH.]

recognition of protein/DNA relative to that of protein/TNS. The highly rigid H1-DNA complex and the strong binding in the recognition of DNA by the protein H1 are perhaps key features in the sealing of the linker DNA during the nucleosome formation.

### Specific protein-DNA interaction

In this section, we will highlight some of the important aspects of specific protein-DNA interaction. The

conformational dynamics, interfacial water dynamics at protein-DNA interface and the possibility of electron transfer will also be reviewed.

### Differential picosecond-resolved dynamics of $\lambda$ -repressor protein upon complexation with different operator DNAs (28)

$\lambda$ -Repressor-operator sites interaction, particularly  $O_R1$  and  $O_R2$ , is a key component of the  $\lambda$ -genetic switch and is a

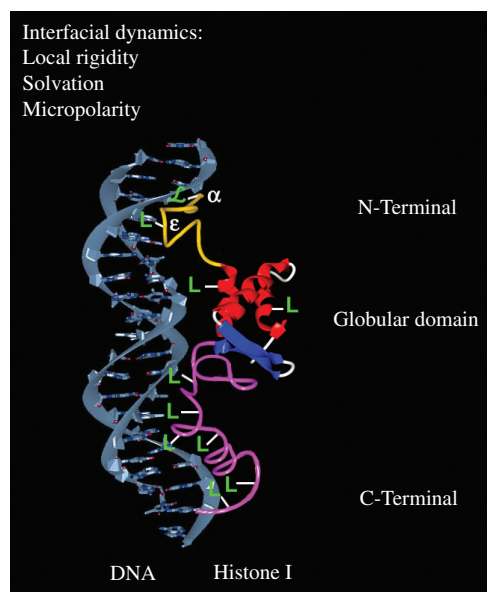


**Figure 9** Model of the interaction between the protein H1 and DNA, showing the interfacial dynamics studied through the covalent and noncovalent labeling of ligands ( $\epsilon$  and L) to the protein.

[Reprinted with permission from ref. (17) Copyright 2001, Wiley-VCH-Verlag GmbH.]

model system for understanding the chemical principles of complex biomolecular recognition. Structurally  $\lambda$ -repressor is a two domain protein as represented in Figure 10. The N-terminal domain interacts with the DNA (16), while

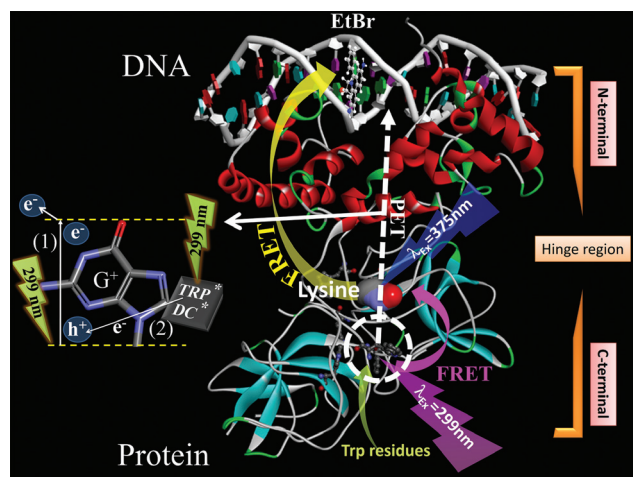


**Figure 10** X-ray crystal structure of  $\lambda$ -repressor bound to operator DNA depicting the simultaneous occurrence of Förster resonance energy transfer (FRET) from tryptophan residues to dansyl, bound to lysine near the C-terminal domain, and from dansyl to EtBr, bound to the operator DNA.

Tryptophan residues were excited at 299 nm and dansyl moiety was excited at 375 nm. The possibility of photoinduced electron transfer (PET) from tryptophan and dansyl (bound to lysine in the protein) to guanine radical or cation in the operator DNA is represented schematically.

C-terminal domain is responsible for most protein-protein interactions (23); these interactions are essential for the co-operative binding (24, 25) and for the functioning of the genetic switch (11, 26). We will discuss the conformational change of the repressor protein and the key dynamical time-scales involved in such specific protein-DNA interactions (28). Though the  $\lambda$  repressor has two cysteine residues, they are all unreactive under native conditions and hence are unsuitable for attaching fluorescent probes (45). Dansylation was carried out for specific covalent fluorescence labeling of the  $\lambda$ -repressor, essentially at the C-terminal region (46) in order to monitor the change in dynamical flexibility upon complexation with two operators DNA,  $O_{R1}$  and  $O_{R2}$ . The picosecond-resolved Förster resonance energy transfer (FRET) technique was used to confirm the location of the dansyl probe with respect to the tryptophan residues of the protein. The tryptophan-dansyl FRET in the protein upon complexation with unlabeled operator DNA was also employed to monitor significant intra-protein structural rearrangement in the C-terminal domain of the protein. As evidenced from Figure 11(A), faster fluorescence transient of tryptophan residues detected at 350 nm (excitation 299 nm) in dansyl-modified  $\lambda$ -repressor compared to that of unmodified  $\lambda$ -repressor, is an indication of the FRET from tryptophan to dansyl moiety. The temporal decay of the tryptophan residues in dansyl-modified repressor shows three time components, including a faster time component of 0.15 ns (45%) unlike unmodified repressor (two longer time components) and as a consequence the average lifetime of tryptophan decreases from 2.8 ns in  $\lambda$ -repressor to 1.37 ns in dansyl-modified repressor. The efficiency of energy transfer is found to be 50%. Both the estimated Förster distance ( $R_0$ ) and donor (tryptophan)-acceptor (dansyl) distance are estimated to be 14.5 Å. Upon addition of unlabeled  $O_{R1}$  and  $O_{R2}$  DNA to the dansylated repressor, an additional faster component of 20 ps appears in the fluorescence transient of tryptophan detected at 350 nm, which is depicted by Figure 11(A) and Figure 11(B), respectively. It has to be noted that the control experiment on the tryptophan emission transients from unlabeled repressor with the operator DNA at 350 nm does not show any faster component, revealing an insignificant possibility of perturbation of tryptophan emission transients in the presence of operator DNA due to other non-radiative processes. The donor (tryptophan)-acceptor (dansyl) distances in dansyl-modified  $\lambda$ -repressor- $O_{R1}$ / $O_{R2}$  DNA complexes are estimated to be 11 Å and 11.8 Å, respectively. Thus, the faster decay of tryptophan in the dansylated  $\lambda$ -repressor with  $O_{R1}$  and  $O_{R2}$  DNA distinctly indicates a significant structural modification in the C-terminal domain, leading to much shorter dansyl-tryptophan distance in the complex. The study also explored FRET from dansyl

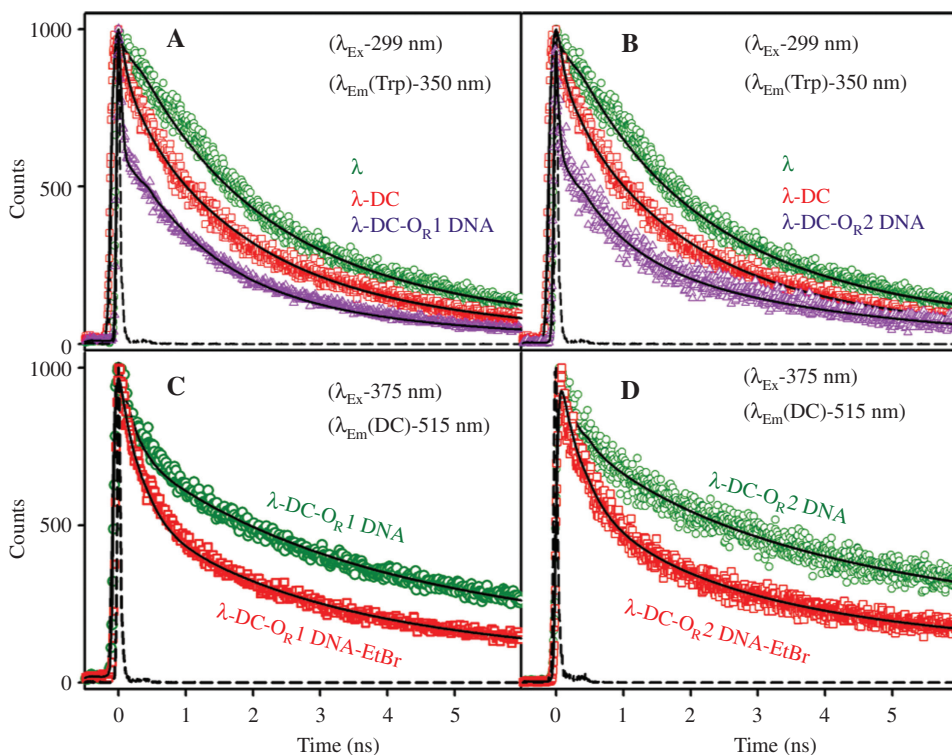


**Figure 11** FRET studies in operator-repressor complexes.

(A) Picosecond-resolved fluorescence transients of tryptophan residues in  $\lambda$ -repressor ( $\lambda$ , green), in dansyl-modified  $\lambda$ -repressor ( $\lambda$ -DC; red) and in dansylated  $\lambda$ -repressor- $O_{R1}$  DNA complex ( $\lambda$ -DC- $O_{R1}$  DNA, violet). Excitation and emission wavelengths were 299 nm ( $\lambda_{\text{ex}}$ -299 nm) and 350 nm [ $\lambda_{\text{em}}$ (Trp)-350 nm], respectively. (B) Picosecond-resolved fluorescence transients of tryptophan residues in  $\lambda$ -repressor ( $\lambda$ ; green), in dansyl-modified  $\lambda$ -repressor ( $\lambda$ -DC; red) and in dansylated  $\lambda$ -repressor- $O_{R2}$  DNA complex ( $\lambda$ -DC- $O_{R2}$  DNA; violet). Excitation and emission wavelengths were 299 nm ( $\lambda_{\text{ex}}$ -299 nm) and 350 nm [ $\lambda_{\text{em}}$ (Trp)-350 nm], respectively. (C) Picosecond-resolved fluorescence transients of dansyl in  $\lambda$ -repressor- $O_{R1}$  DNA complex in absence ( $\lambda$ -DC- $O_{R1}$  DNA, green) and in presence ( $\lambda$ -DC- $O_{R1}$  DNA-EtBr, red) of EtBr. Excitation and emission wavelengths were 375 nm ( $\lambda_{\text{ex}}$ -375 nm) and 515 nm [ $\lambda_{\text{em}}$ (DC)-515 nm], respectively. (D) Picosecond-resolved fluorescence transients of dansyl in  $\lambda$ -repressor- $O_{R2}$  DNA complex in absence ( $\lambda$ -DC- $O_{R2}$  DNA; green) and in presence of EtBr ( $\lambda$ -DC- $O_{R2}$  DNA-EtBr; red). Excitation and emission wavelengths were 375 nm ( $\lambda_{\text{ex}}$ -375 nm) and 515 nm [ $\lambda_{\text{em}}$ (DC)-515 nm], respectively. [Reprinted with permission from ref. (28) Copyright 2011, Elsevier B.V.]

chromophore in the repressor protein to the operator DNA-bound EtBr in the protein-DNA complex. Steady-state emission quenching and enhancement of dansyl and ethidium, respectively, in the complex and the faster fluorescence decay of dansyl in dansyl-modified  $\lambda$ -repressor- $O_{R1}/O_{R2}$  DNA-EtBr complexes (Figure 11C and Figure 11D, respectively) at 515 nm are the indicative of the resonance energy transfer. The efficiency of energy transfer from dansyl to EtBr in  $\lambda$ -repressor- $O_{R2}$  DNA-EtBr complex (48%) is higher than in  $\lambda$ -repressor- $O_{R1}$  DNA-EtBr complex (29%). The dansyl-ethidium distances in  $\lambda$ -repressor- $O_{R1}/O_{R2}$  DNA-EtBr complexes are estimated to be 24 Å and 20 Å, respectively, indicating that the structure of the protein is more compact in the  $O_{R2}$  complex than in the  $O_{R1}$  complex.

Polarization gated fluorescence anisotropy decay profiles of dansyl in  $\lambda$ -repressor and in  $\lambda$ -repressor-operator DNA complexes are shown in Figure 12. The rotational flexibility of the protein before and after complexation with

operator DNA is investigated by time-resolved fluorescence anisotropy studies. The fluorescence anisotropy,  $r(t)$ , which can decay in time because of the rotational motion of the molecules and consequently leads to depolarization of the fluorescence is fitted to biexponential decay function. The faster time constant indicates the local/inertial motion of the probe and the slower one reveals the overall tumbling motion of the entire protein (47). The estimated rotational time constant ( $\tau$ ) for the repressor associated with the overall  $\lambda$ -repressor tumbling is estimated to be 27 ns using the Stokes-Einstein-Debye (SED) equation (48). The numerical fitting of the fluorescence anisotropy decay transient (Figure 12A), the longer time constant to be 27 ns was kept constant. In the case of  $\lambda$ -repressor, the obtained faster time constant of 800 ps provides a quantitative measure of the flexibility of the lysine-bound dansyl in the C-terminal domain. Upon complexation with the  $O_{R1}$  and  $O_{R2}$  DNA, the faster time components become 370 ps

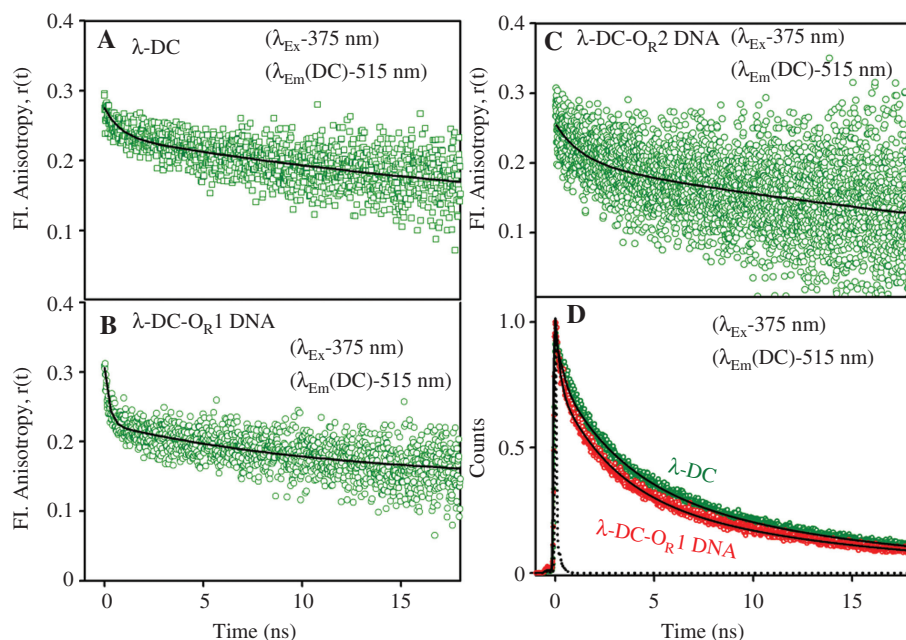


**Figure 12** Fluorescence anisotropy,  $r(t)$  of (A) dansyl in  $\lambda$ -repressor ( $\lambda$ -DC; green), (B) dansyl in  $\lambda$  repressor- $O_R1$  DNA complex ( $\lambda$ -DC- $O_R1$  DNA; green), (C) dansyl in  $\lambda$ -repressor- $O_R2$  DNA complex ( $\lambda$ -DC- $O_R2$  DNA; green), (D) picosecond-resolved fluorescence transients of dansyl in  $\lambda$ -repressor ( $\lambda$ -DC; green) and in  $\lambda$ -repressor- $O_R1$  DNA complex ( $\lambda$ -DC- $O_R1$  DNA; red). Excitation and emission wavelengths were 375 nm ( $\lambda_{Ex}-375 \text{ nm}$ ) and 515 nm [ $\lambda_{Em}(DC)-515 \text{ nm}$ ] for all the systems, respectively. [Reprinted with permission from ref. (28) Copyright 2011, Elsevier B.V.]

and 1.3 ns, respectively. The observation clearly indicates that the flexibility in the C-terminal domain of the protein upon complexation with the  $O_R1$  DNA is much higher compared to that of the  $O_R2$  DNA (Figure 12B,C). The faster fluorescence decay of dansyl probe in  $\lambda$ -repressor upon interaction with the  $O_R1$  DNA is evident from Figure 12(D). The flexibility of the dansyl probe leading to its exposure to the aqueous environment is also evident from the time-resolved decay [faster decay due to the TICT process (49)] of the probe upon interaction with the  $O_R1$  DNA (Figure 12D), and as a consequence, the average lifetime of dansyl decreases from 5.56 ns in dansyl-modified  $\lambda$ -repressor to 3.48 ns in dansyl-modified repressor- $O_R1$  DNA complex. On the contrary, the dansyl in the  $\lambda$ -repressor- $O_R2$  DNA complex shows insignificant change (data not shown) in the fluorescence decay compared to that of the free protein indicating less flexibility in the C-terminal domain, which is consistent with the anisotropy study.

#### Interfacial picosecond-resolved solvation dynamics of specific protein-DNA complexes: $\lambda$ -repressor with different operator DNAs (31)

What role does the interfacial water molecules play in determining the specificity of association, is a critical

question. In this section, we discuss the dynamical role of minor groove water molecules and DNA side chain flexibility in a lambda repressor-operator DNA interaction using well-characterized DNA minor groove binder dye, Hoechst33258 (31). Figure 13 shows emission spectra of Hoechst33258 (H258) bound to different operators DNA in the presence and absence of  $\lambda$ -repressor. In the presence of  $O_R1$  and  $O_R2$  DNA, the emission maximum of H258 (buffer: 500 nm) is significantly blue shifted ( $O_R1$  DNA: 457 nm,  $O_R2$  DNA: 460 nm) because of the interaction of H258 with DNA. Upon addition of  $\lambda$ -repressor to the H258, bound to operator DNA, the emission spectrum is further blue shifted especially in H258- $O_R2$ - $\lambda$  complex as shown in Figure 13(B). The possibility of nonspecific binding of repressor protein with H33258 was ruled out from a time-resolved experiment. Time-resolved polarization gated fluorescence anisotropy analysis (Figure 13D) further supports the observation as the rotational time constant ( $\tau_{rot}$ ) of H258 in absence and in presence of  $\lambda$ -repressor remains unaltered ( $\tau_{rot}=0.55 \text{ ns}$ ). In the DNA-protein complex, the anisotropy decay pattern of H258 remains unaltered, suggesting the location of the probe in DNA does not change even after the complex formation. The representative anisotropy decay of H258 in DNA-protein complex is shown in Figure 13(H). In order to investigate conformational and structural changes of the operator DNA, upon interaction

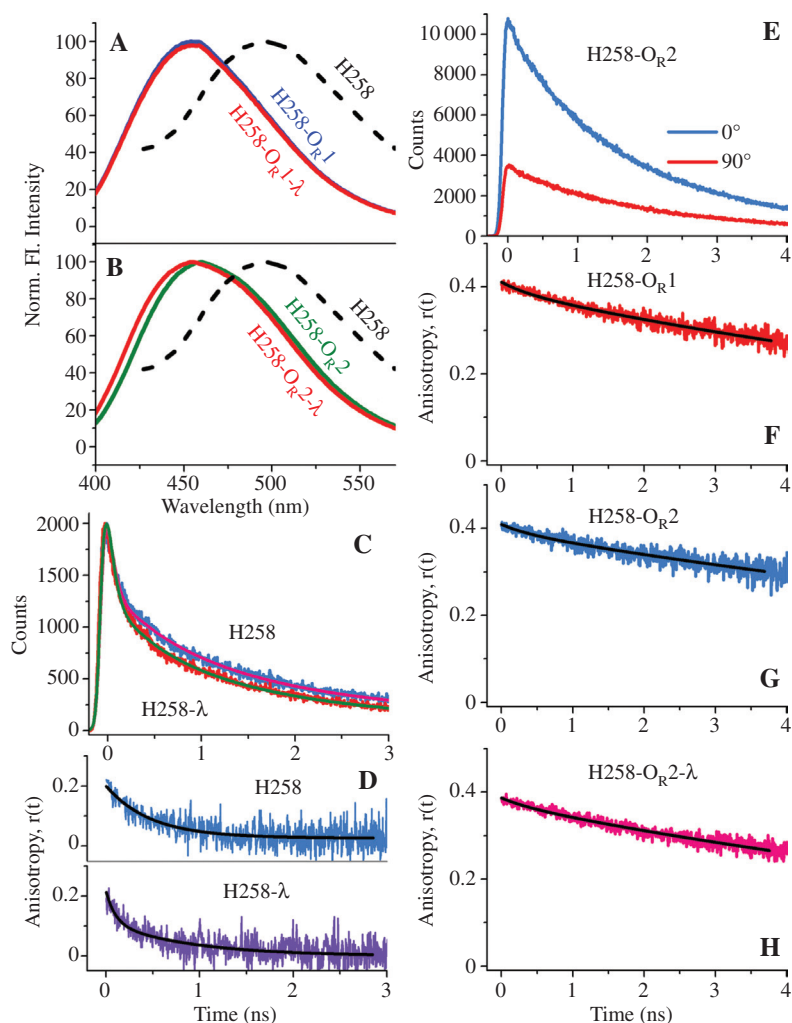


**Figure 13** Normalized steady-state fluorescence spectra of probe H258 in three different environments.

(A) In buffer,  $O_{R1}$  DNA and  $O_{R1}$ -repressor complex. (B) In buffer,  $O_{R2}$  DNA and  $O_{R2}$ -repressor complex. (C) Picosecond-resolved fluorescence transients of H258 is shown in presence  $\lambda$ -repressor protein. For comparison, the fluorescence transient of H258 in buffer solution is also included. (D) Time-resolved fluorescence anisotropies,  $r(t)$ , of the probe in water (buffer) and in presence  $\lambda$ -repressor protein at emission wavelength of 500 nm are shown. (E) Representative time-resolved traces of H258 in  $O_{R2}$  at different polarization ( $0^\circ$  and  $90^\circ$ ) is shown. Time-resolved fluorescence anisotropies of H258 in  $O_{R1}$  (F) and  $O_{R2}$  (G) are depicted. (H) Represents the anisotropy decay of H258 in  $O_{R2}$ -protein complex. [Reprinted with permission from ref. (31) Copyright 2013, Elsevier B.V.]

with  $\lambda$ -repressor, CD spectroscopy was used. Figure 14 represents the CD spectra of operator DNA,  $O_{R1}$  and  $O_{R2}$  in the absence and in the presence of  $\lambda$ -repressor. In the case of  $O_{R2}$  (Figure 2B), careful observation reveals a shift of the spectral maximum (270 nm) along with the increase in ellipticity upon complexation with  $\lambda$ -repressor. In the case of  $O_{R1}$  DNA (Figure 14A), a negligible spectral shift and a smaller change in ellipticity was observed in comparison to  $O_{R2}$ . The observation indicates the conformational change of  $O_{R2}$  after binding to the repressor is significant compared to that of  $O_{R1}$ . The time-resolved fluorescence transients are represented in Figure 15(B). As evident, from Figure 15(B; lower panel), upon addition of repressor to  $O_{R2}$ , the efficiency of energy transfer from H258 to EtBr

decreases (72% to 59%), whereas in case of  $O_{R1}$  (upper panel), the efficiency remains unaltered (57%). The FRET study clearly demonstrates that  $O_{R2}$  DNA undergoes significant conformation change upon protein binding, leading to the decrease in energy transfer efficiency. The observation corroborates the findings of the CD study, which also indicates the structural changes within  $O_{R2}$  DNA. For a better understanding of the energy transfer from the excited state of H258 to EtBr molecules, it is imperative to know the distribution of acceptor (EtBr) molecules within the DNA, as it is a governing factor that can influence the energy transfer rate as observed from the time-resolved fluorescence studies (50). In this context, a kinetic model developed by Tachiya (51) for the

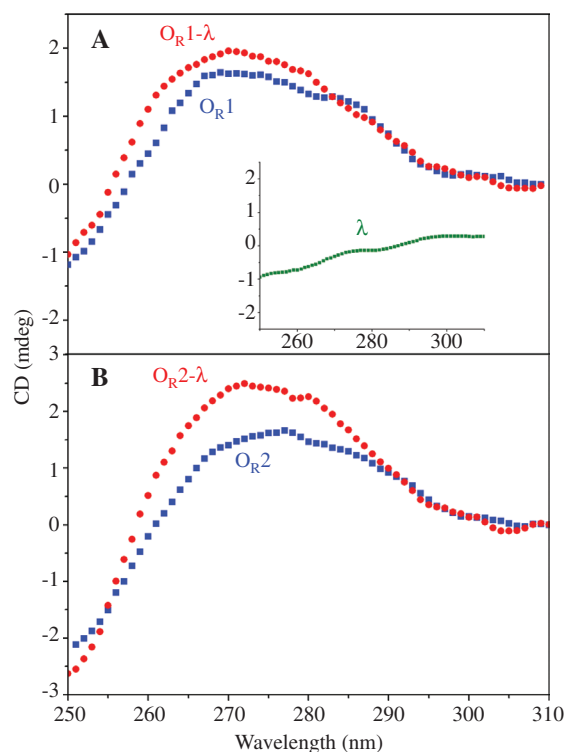


**Figure 14** Circular dichroism (CD) spectroscopy of operators and their complexes with repressor protein.

(A) Ellipticity (mdeg) of  $O_{R1}$  DNA in presence and in absence of  $\lambda$ -repressor protein. The inset image represents the CD spectrum of  $\lambda$ -repressor protein. (B) Depicts the optical rotation (mdeg) of  $O_{R2}$  DNA in presence and in absence of  $\lambda$ -repressor protein. Upon complexation with protein, the characteristic peak of DNA around 270 nm is blue shifted. No significant wavelength shift was observed in case of  $O_{R1}$ . [Reprinted with permission from ref. (31) Copyright 2013, Elsevier B.V.]

quenching of luminescent probes undergoing non-radiative energy transfer in restricted environments was applied. In contemporary literature, the kinetic model finds its relevance in various aspects including drug binding (52) and nanoparticles quenching (53). In the current study, the host is the DNA strand itself, where EtBr intercalates. For  $O_{R1}$  DNA (Figure 15C), the mean number ( $m$ ) of intercalated ethidium moiety present per DNA was estimated to be  $\sim 5$  and the quenching rate constant ( $k_q$ ) was estimated 0.9/ns. The  $m$  and  $k_q$  values remain unchanged in DNA-protein complex. In the case of  $O_{R2}$  (Figure 15C), the mean number of acceptor (ethidium) per DNA was estimated to be  $\sim 6$  and the quenching constant was 1.4/ns. Upon the addition of repressor, the quenching rate constant for  $O_{R2}$  decreases to a value of 1.1/ns. In order to get an idea of the probability distance distribution, we analyzed the time-resolved fluorescence decays of DNA-bound H258 in presence and absence of EtBr to construct the distance distribution function,  $P(r)$  (30). The half width (hw) of the distance distribution changes from 3.5 Å

(H258- $O_{R2}$ -EtBr) to 3 Å (H258- $O_{R2}$ -EtBr- $\lambda$ ) as shown in Figure 15(D) (31). In the case of  $O_{R1}$ , the distance distribution between H258 and EtBr does not change in the presence of protein. The local dynamics of water molecules, actively take part in various biological functions including the recognition process as well as in maintaining the biological activity (28). As revealed by the various structural studies, H258 remains attached to the both the repressor bound and unbound operator DNA and hence can report their environmental dynamics. Figure 16(A) displays the fluorescence transients (blue to red end) of H258 in  $O_{R1}$  DNA, in the absence and in the presence of  $\lambda$ -repressor. Figure 16(B) shows the constructed TRES of H258 giving a shift of 1300/cm and 1450/cm in a 10 ns time window for  $O_{R1}$  and  $O_{R1}$ -repressor complex, respectively, which indicates that H258 in the excited state is stabilized because of the solvation by the minor groove water molecules along with the DNA itself. However, the change in the net spectral shift of H258 for  $O_{R1}$  and  $O_{R1}$  repressor complex is insignificant. The corresponding solvation correlation decay profiles are presented in the inset image. The solvation correlation decay profile of H258 in  $O_{R1}$ , consists of the decay time constant of 50 ps (35%) and 7 ns (65%). One of the previous femtosecond-resolved studies on the DNA minor groove water dynamics reveals the hydration time scale of 1.4 ps and 20 ps (35). However, in the limited time resolution (picosecond resolved), the observed 50 ps component in the solvation decay profile is consistent with the sub-100-picosecond relaxation of minor groove water molecules (36). The major decay component of  $\sim 10$  ns is related to the relaxation of the DNA structure itself (36). The observed solvation decay constants of H258 are consistent with our earlier studies (54). Strikingly, the constructed solvation correlation decay for H258 in DNA-protein complex does not change significantly as shown in Figure 16(A) [50 ps (30%) and 7 ns (70%)]. Figure 17A displays the fluorescence transients of H258 from the blue to the red end, i.e., 410 nm, 470 nm, and 530 nm in  $O_{R2}$  and  $O_{R2}$ -repressor complex. At the blue edge of the spectrum, the fluorescence transient decays on much faster time scales compared to the transients collected at the red end. Figure 5(B) shows the constructed TRES giving a shift of 1200/cm and 1350/cm in a 10 ns time window for  $O_{R2}$  and  $O_{R2}$ -repressor complex, respectively, essentially indicating that the probe H258 in the excited state is stabilized because of the solvation. As represented in Figure 18(A), the solvation correlation decay function of H258 in  $O_{R2}$  at room temperature consists of time constants of 50 ps (30%) and 9.0 ns (70%). In the presence of  $\lambda$ -repressor (Figure 18B), the time constant changes to 80 ps (30%) and 11 ns (70%). The unaltered net spectral shift for both

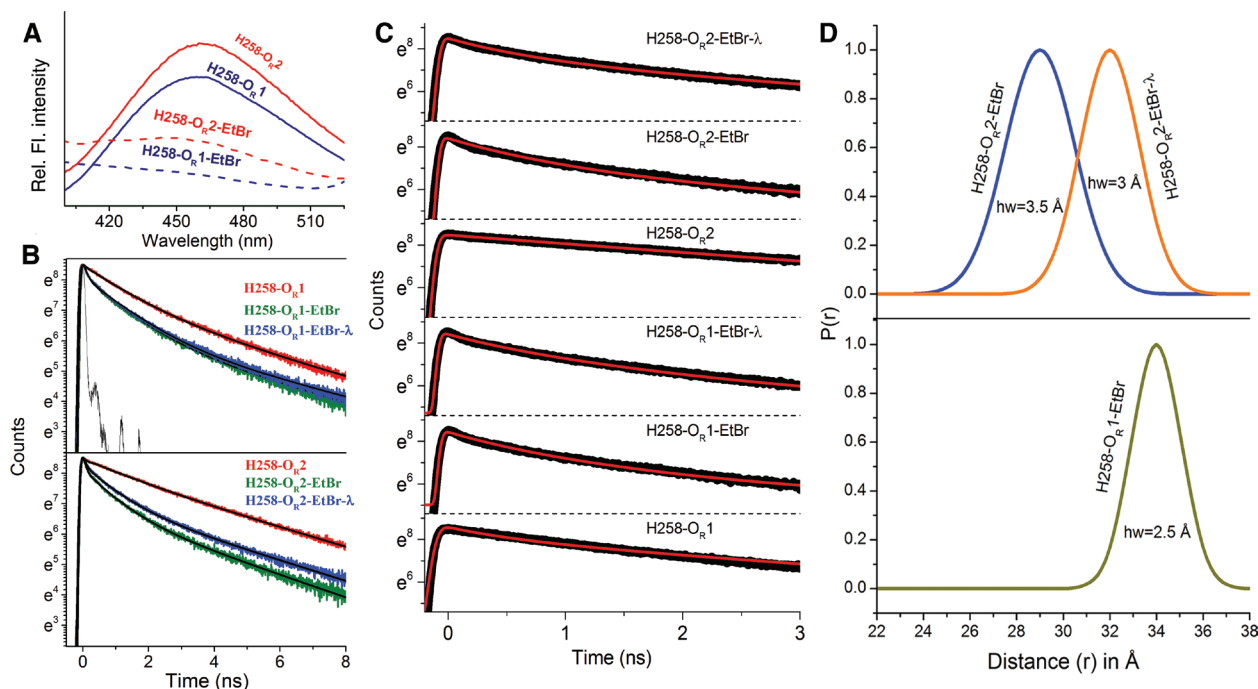


**Figure 15** Steady-state and time-resolved FRET quenching and Tachiya kinetic model analysis.

(A) Steady-state emission spectra of H258 in operator DNA in presence and in absence of EtBr. (B) The fluorescence lifetime quenching of H258. Upper panel shows the effect of EtBr in O<sub>R</sub>1 system and the lower panel depicts the energy transfer for O<sub>R</sub>2 system. (C) Fitting of time-resolved lifetime data of H258 under various conditions by Tachiya kinetic model. (D) Probability of distance distribution (P(r)) with respect to mean donor-acceptor distance.

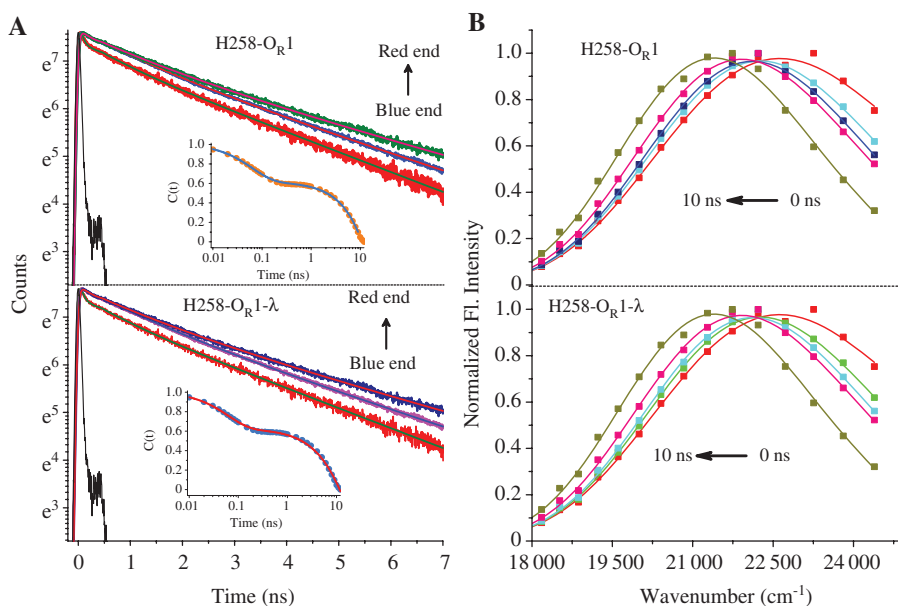


**Figure 16** Solvation relaxation of H258 in O<sub>R</sub>1 and O<sub>R</sub>1-repressor complex.

(A) Picosecond-resolved fluorescence transients of H258 at three wavelengths in O<sub>R</sub>1 DNA and O<sub>R</sub>1-repressor complex respectively are shown. The excitation wavelength was 375 nm. Solid lines indicate exponential numerical fitting of the experimental data points. The insets depict the solvation correlation decay profiles of H258 in O<sub>R</sub>1 in absence and in presence of lambda repressor. (B) Time-resolved emission spectrum (TRES) of H258 in O<sub>R</sub>1 and O<sub>R</sub>1-repressor complex are shown, respectively. The lifetime plots are in semi-log format to better visualize the change of the lifetime traces at different wavelengths. [Reprinted with permission from ref. (31) Copyright 2013, Elsevier B.V.]

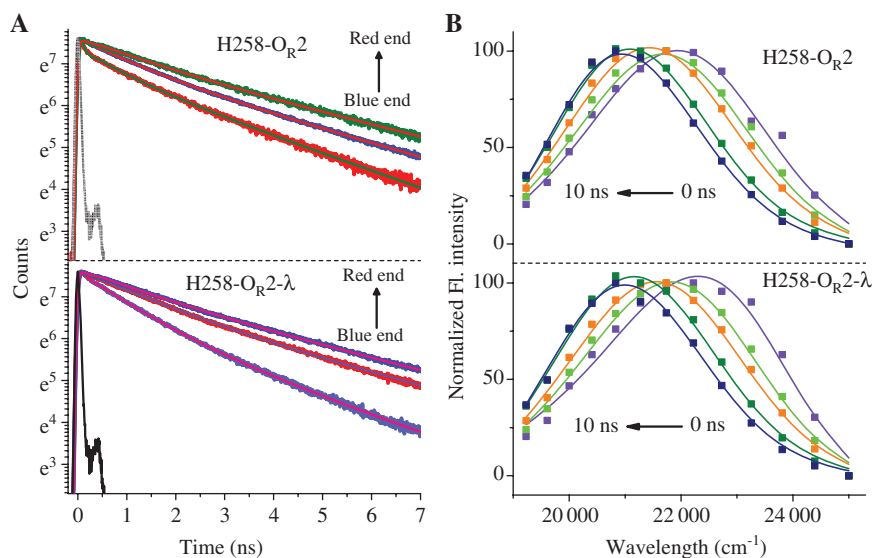


**Figure 17** Solvation relaxation of H258 in  $O_{R2}$  and  $O_{R2}$ -repressor complex.

(A) Picosecond-resolved fluorescence transients of H258 at three wavelengths in  $O_{R2}$  DNA and  $O_{R2}$ -repressor complex respectively are shown. The excitation wavelength was 375 nm. Solid lines indicate exponential numerical fitting of the experimental data points. (B) Time-resolved emission spectrum (TRES) of H258 in  $O_{R2}$  and  $O_{R2}$ -repressor complex are shown, respectively. The lifetime plots are in semi-log format to better visualize the change of the lifetime traces at different wavelengths. [Reprinted with permission from ref. (31) Copyright 2013, Elsevier B.V.]

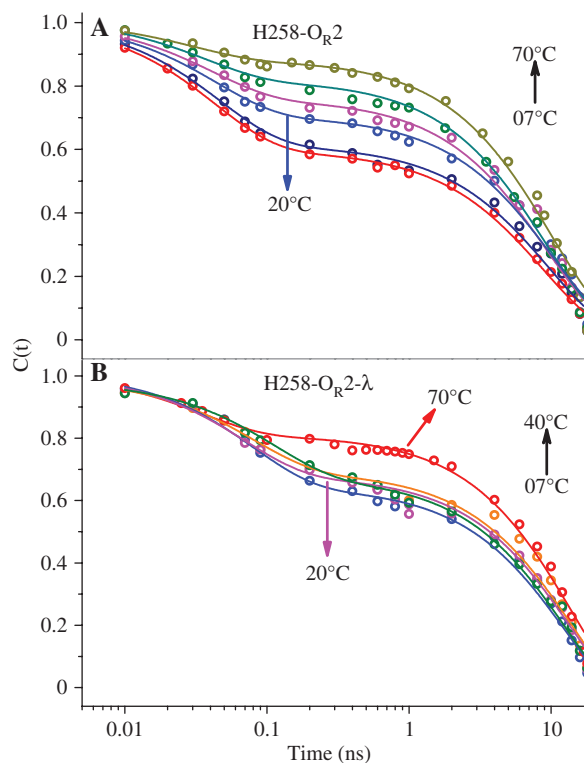


**Figure 18** Temporal decay of the solvation correlation function  $[C(t)]$  at different temperatures for the H258 in (A)  $O_{R2}$  and in (B)  $O_{R2}$ -repressor complex.

The time has been plotted on a logarithmic scale. Solid lines indicate exponential fitting of the experimental data points. [Reprinted with permission from ref. (31) Copyright 2013, Elsevier B.V.]

DNA and DNA-protein complex is consistent with similar solvation correlation decay profile. Negligible change in the faster time scale of the solvation decay profile is observed, suggesting less perturbed water dynamics in the minor groove of DNA ( $O_{R1}/O_{R2}$ ) in the presence of repressor. In the case of  $O_{R2}$ , the DNA side chain flexibility is slightly hindered as reflected in the slower decay component (9.0 ns changes to 11 ns). However, in the case of  $O_{R1}$ , upon repressor binding, side chain flexibility remains unchanged as reflected in the H258 solvation decay profile. Upon repressor binding, the slight change in the slower decay component of H258 solvation decay profile in the case of  $O_{R2}$ , could be attributed to the observed conformational change of its structure upon protein binding. In this context, it is important to understand whether exchange of minor groove water with the bulk water decreases due to the formation of a stable interface in the DNA-protein complex. In order to address exchange of minor groove water with the bulk water, a temperature-dependent TRES analysis of H258 in operator DNA in absence and presence of repressor was carried out. Figure 18(A) shows the temporal decay of the solvation correlation function  $[C(t)]$  for the probe (H258) bound to  $O_{R2}$  at various temperatures. At a lower temperature ( $7^\circ$ ), the solvation correlation function decays with a time constant of 40 ps (40%) and 9 ns (60%). With an increase in temperature, the contribution of faster solvation decay time gradually decreases and the overall solvation becomes slower.

At 40°C, the temporal decay of the solvation correlation function shows time constants of 40 ps (20%) and 9 ns (80%). On the contrary, for  $O_R2$ -repressor complex, the temperature-dependent hydration dynamics follows a different course (Figure 18B). The solvation correlation profile decays with a time constant of 100 ps (30%) and 12.3 ns (70%) at lower temperature (7°C). In the temperature region of 7–40°C, the water dynamics in the repressor-operator interface is minimally affected as reflected in the solvation correlation decays (Figure 18B). With further increments of temperature, >50°C, the water dynamics around H258 changes significantly, possibly because of the melting of the DNA strand itself.

The temperature-dependent solvation studies unearth the exchangeability of minor groove water molecules with the bulk water molecules. In the free operator DNA, the exchangeability of minor groove changes with increase in temperature as reflected in the faster solvation decay time. However, because of the formation of a stable interface in the DNA-protein complex, the water molecules in the minor groove are conserved and less susceptible to the temperature changes.

### Differential electron transfer dynamics in specific protein-DNA complexes (27)

Ultrafast electron transfer phenomenon in protein and protein-DNA complex is crucial and often leads to the regulation of various kinds of redox reactions in biological macromolecules. Although the conformation of protein in protein-DNA complex plays the key role in the electron transfer process, until now very little evidence exists in the literature.  $\lambda$ -Repressor-operator DNA interaction, particularly  $O_R1$  and  $O_R2$ , is a key component of the  $\lambda$ -genetic switch and is a model system for understanding the chemical principles of the conformation dependent electron transfer reaction, governed by differential protein dynamics upon binding with different DNA target sequences. In this section, we will discuss the photoinduced electron transfer (PET) from the tryptophan moieties of the protein  $\lambda$ -repressor to two operators of DNA of different sequences using picosecond-resolved fluorescence spectroscopy.

Figure 19(A) shows the diffusion-controlled complexation of  $\lambda$ -repressor with operator DNA ( $O_R1$ ) with increasing time. The snapshots represent the interfacial region of the reactant fluids, i.e.,  $O_R1$  DNA intercalated with EtBr and dansylated  $\lambda$ -repressor. The green and red fluorescence represent the emission of dansyl-modified  $\lambda$ -repressor and EtBr bound to DNA inside the microfluidics channel, respectively. The decrease in the blue fluorescence

intensity with time (up to 70 s) is an indication of energy transfer from dansyl in the protein to DNA-bound EtBr (Figure 19C). The control experiment is done using dansylated  $\lambda$ -repressor and phosphate buffer as a reference to consider the dilution effect on the fluorescence intensity of dansyl-modified  $\lambda$ -repressor upon mixing. Within a smaller time frame (Figure 19D), the blue fluorescence intensity for the reference system changes insignificantly in comparison to the dansylated  $\lambda$ -repressor-DNA-EtBr complex, which confirms the occurrence of FRET as mentioned above. Moreover, for the system under investigation, the diffusion of the biomolecules with increasing time is also monitored and represented in Figure 19(B). The diffusion coefficient is calculated to be 86.7/ $\mu\text{m}^2/\text{s}$ . The steady-state absorption spectra of DNA, dansylated  $\lambda$ -repressor, and the emission spectra of  $\lambda$ -repressor before (excitation 299 nm) and after (excitation 375 nm) dansylation, are shown in Figure 19E. The emission spectrum of tryptophan in  $\lambda$ -repressor shows a distinct peak at 350 nm upon excitation at 299 nm, which becomes significantly quenched after binding with operator DNA as is evident from Figure 19(F). The decrease in steady-state fluorescence of tryptophan in  $\lambda$ -repressor upon binding to operator DNA reflects PET from tryptophan to DNA, as already reported for some different biological systems in the literature. The emission spectrum of dansyl-modified  $\lambda$ -repressor-DNA complex shows a peak at 515 nm (excitation at 375 nm), which is found to be significantly quenched when excited at 299 nm, as shown in Figure 19(F). It should be noted that the optical density at both the excitation wavelengths (299 nm and 375 nm) are similar (Figure 19E). The reduced fluorescence intensity of dansyl in dansyl-modified  $\lambda$ -repressor-DNA complex at 299 nm excitation compared to that at 375 nm excitation wavelength could also be an indicative of ET reaction from dansyl to operator DNA at the excitation wavelength of 299 nm. In Figure 20(A), the fluorescence transients of tryptophan residues within  $\lambda$ -repressor in presence and absence of  $O_R1$  DNA are shown. The  $\lambda$ -repressor monomer contains three tryptophan residues at position W129, W142 and W230. The latter two are in the C-terminal domain while the first one is in the hinge region. The tryptophan fluorescence within  $\lambda$ -repressor at all the detected wavelengths (330 nm, 350 nm and 380 nm) in the absence of the operator DNA depicts similar decay profiles, revealing similar environments around the tryptophan residues, which is evident from the insignificant change in the lifetime of tryptophan at these wavelengths. However, in the presence of the  $O_R1$  DNA, although the fluorescence transient of tryptophan at 350 nm remains essentially unaltered, the decay profiles at 330 nm and 380 nm become significantly faster (Figure

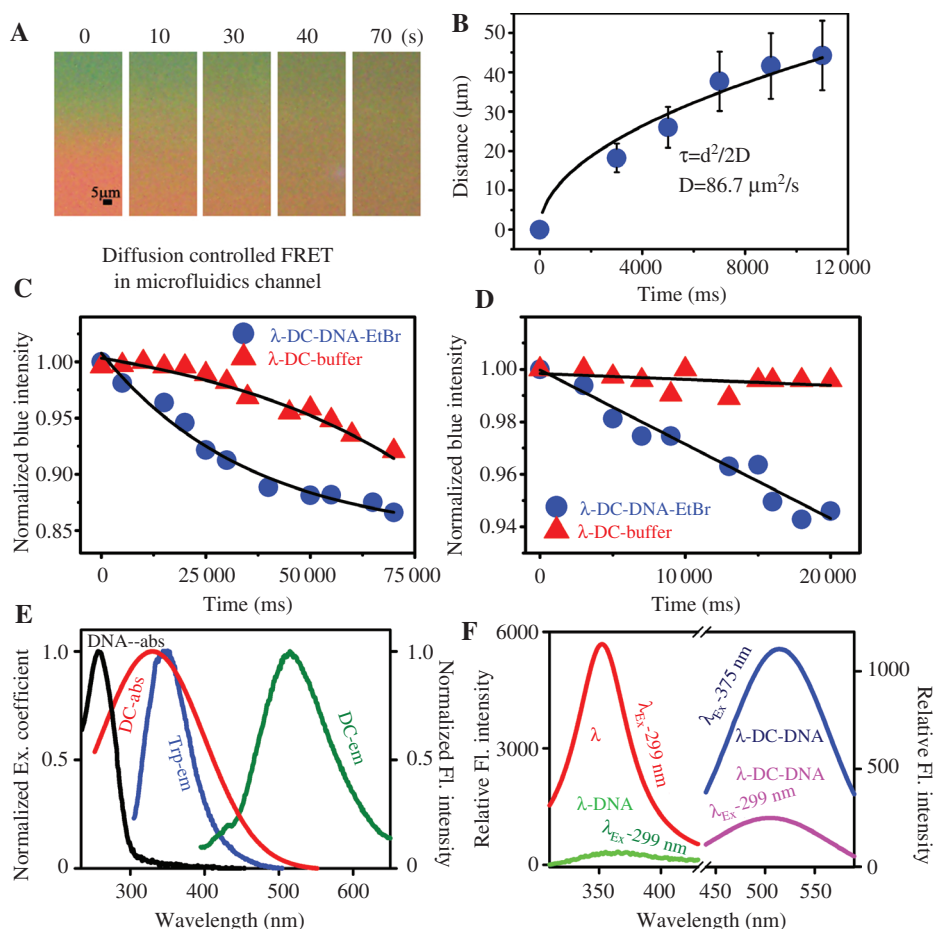
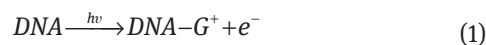


**Figure 19** Diffusion-controlled FRET in microfluidics channel.

(A) Fluorescence microscopic images of dansylated  $\lambda$ -repressor- $O_R1$  DNA-EtBr complex at a fixed position of microfluidics channel in different time window. (B) Diffusion of the biomolecule (dansylated  $\lambda$ -repressor) under study. (C) Change in normalized blue intensity of dansylated  $\lambda$ -repressor in buffer ( $\lambda$ -DC-buffer; red) and dansylated  $\lambda$ -repressor- $O_R1$  DNA-EtBr complex ( $\lambda$ -DC-DNA-EtBr) with time (up to 70 s). (D) Same as described in (C) within a smaller time window (20 s). (E) The steady-state absorption spectra of DNA (DNA-abs; black), Dansyl (DC-abs; red), and emission spectra of tryptophan in  $\lambda$ -repressor (Trp-em; blue), dansyl bound to  $\lambda$ -repressor (DC-em; green) are shown. (F) Steady-state fluorescence spectra of tryptophan in  $\lambda$ -repressor ( $\lambda$ ; red) and in  $\lambda$ -repressor- $O_R1$  DNA complex ( $\lambda$ -DNA; green). Systems are excited at 299 nm. Steady-state fluorescence spectra of dansyl in  $\lambda$ -repressor- $O_R1$  DNA complex at excitation wavelength 375 nm ( $\lambda$ -DC-DNA; blue) and 299 nm ( $\lambda$ -DC-DNA; pink) are shown. [Reprinted with permission from ref. (27) Copyright 2012, Taylor & Francis.]

20A), revealing a faster time constant of  $\sim 20$  ps. The observation clearly reveals a non-radiative channel for the buried (emitting at the blue end of the tryptophan emission spectrum, e.g., 330 nm) and solvent exposed (emitting at the red end of the tryptophan emission spectrum, e.g., 380 nm) tryptophan residues in  $\lambda$ -repressor- $O_R1$  DNA complex. The fluorescence transients of tryptophan residues within  $\lambda$ -repressor in the presence and absence of  $O_R2$  DNA are depicted in Figure 20(A). Although the fluorescence transient of tryptophan at 350 nm, upon addition of  $O_R2$  DNA remains unaltered, the decay profile of tryptophan at 330 nm becomes faster, revealing an ultrafast time constant of  $\sim 20$  ps. We assign the ultrafast non-radiative decay of the tryptophan residues as due to PET. In the

excitation wavelength (299 nm), the possibility of formation of guanyl radicals in the DNA caused by removal of a single electron from guanine cannot be ruled out (55). Therefore, tryptophan (reduction potential of its single electron oxidation product at pH 7 is +1.03 V) that has a lower oxidation potential than guanine (reduction potential of guanosine, +1.29 V), can act as electron donor or hole acceptor, retrieving the native state of guanine from its radical cation (55) (Figure 10). Therefore, the excited state reaction scheme can be given as below:



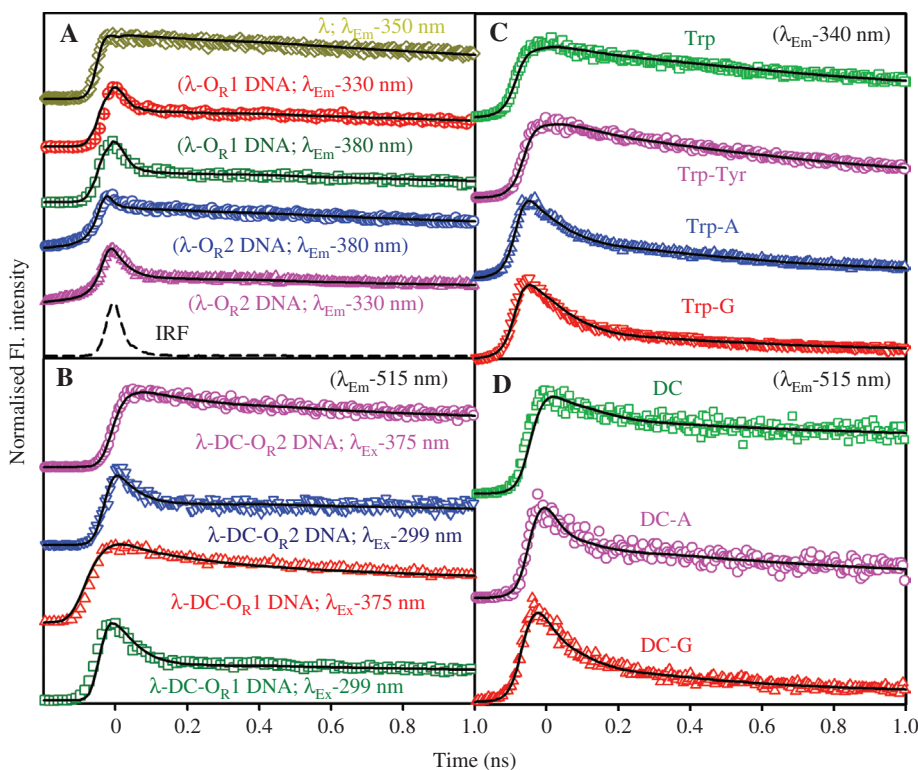


**Figure 20** Excited state charge transfer in operator-repressor complexes.

(A) The Picosecond-resolved fluorescence transients of tryptophan in  $\lambda$ -repressor in absence of DNA detected at 350 nm ( $\lambda$ ;  $\lambda_{em}$ -350 nm; dark yellow), in presence of  $O_{R1}$  DNA detected at 330 nm ( $\lambda$ - $O_{R1}$  DNA;  $\lambda_{em}$ -330 nm; red) and 380 nm ( $\lambda$ - $O_{R1}$  DNA;  $\lambda_{em}$ -380 nm; green) and in presence of  $O_{R2}$  DNA detected at 330 nm ( $\lambda$ - $O_{R2}$  DNA;  $\lambda_{em}$ -330 nm; pink) and 380 nm ( $\lambda$ - $O_{R2}$  DNA;  $\lambda_{em}$ -380 nm; blue). Excitation wavelength is 299 nm. (B) Fluorescence transients of dansyl in  $\lambda$ -repressor- $O_{R1}$  DNA complex, excited at 375 nm ( $\lambda$ -DC- $O_{R1}$  DNA;  $\lambda_{ex}$ -375 nm; red) and at 299 nm ( $\lambda$ -DC- $O_{R1}$  DNA;  $\lambda_{ex}$ -299 nm; green). Fluorescence transients of dansyl in  $\lambda$ -repressor- $O_{R2}$  DNA complex, excited at 375 nm ( $\lambda$ -DC- $O_{R2}$  DNA;  $\lambda_{ex}$ -375 nm; pink) and at 299 nm ( $\lambda$ -DC- $O_{R2}$  DNA;  $\lambda_{ex}$ -299 nm; blue). Emission wavelength is 515 nm ( $\lambda_{em}$ -515 nm). (C) Fluorescence transients of tryptophan only (Trp; green) and tryptophan in presence of adenine (trp-A; blue) and in presence of guanine (Trp-G; red) and in presence of N-acetyl tyrosinamide (Trp-Tyr; pink). Emission and excitation wavelengths are 340 nm and 299 nm, respectively. (D) Fluorescence transients of dansyl (DC; green) and dansyl in presence of adenine (DC-A; pink) and in presence of guanine (DC-G; red) are shown. Emission and excitation wavelengths are 515 nm and 299 nm. [Reprinted with permission from ref. (27) Copyright 2012, Taylor & Francis.]

The estimated the electron transfer rate  $k_{ET}$  for different systems in the following way, (56)

$$k_{ET} = \frac{1}{\tau_{trp-O_{R1}DNA/O_{R2}DNA}} \cdot \frac{1}{\tau_{trp}}, \quad (3)$$

where  $\tau_{trp}$ ,  $\tau_{trp-O_{R1}DNA}$  and  $\tau_{trp-O_{R2}DNA}$  are the average lifetime of tryptophan in  $\lambda$ -repressor and in  $\lambda$ -repressor- $O_{R1}$ / $O_{R2}$  DNA complex, respectively. The electron transfer rate ( $k_{ET}$ ) from tryptophan to  $O_{R1}$  DNA at 330 and 380 nm is found to be  $1.81 \times 10^9/s$  and  $2.4 \times 10^9/s$ , respectively. The ET rate ( $k_{ET}$ ) from tryptophan to  $O_{R2}$  DNA at 330 is found to be  $1.3 \times 10^9/s$ . It has to be noted that the tryptophan residues are about 30 Å away from the DNA surface (estimating the distance, using X-ray crystal structure of  $\lambda$ -repressor-operator DNA complex in VIEWER LITE software). In that case, the tryptophan residues may contribute in the process of

long range ET through space, involving solvent, peptide bridge, or ion pairing to the operator DNA located at the N-terminal domain of the protein (57). The long range ET rates reportedly vary from ultrafast ( $10^{10}/s$ ) to very slow time scale ( $10^3/s$ ) depending on the distance as well as the system under study (57). The long range ET rates observed in our experiment are found to be well within the rates reported in the existing literature.

The structural dissimilarity between the  $O_{R1}$  and  $O_{R2}$  DNA-bound  $\lambda$ -repressor is distinctly evident from the observation. For repressor- $O_{R1}$  DNA complex both the tryptophan residues (water exposed and buried) are participating in the ET reaction. In contrast, for the repressor- $O_{R2}$  DNA complex, only the buried tryptophan residues are responsible for the ET reaction. The observation can be correlated with the dynamical flexibility of the protein upon binding with  $O_{R1}$  DNA compared to that with  $O_{R2}$

DNA. It has to be noted that the flexibility in the C-terminal domain of the protein upon DNA binding is reflected in the electron transfer reactions in the protein-DNA complexes as most of the tryptophan residues reside in the C-terminal domain. The dansyl probe, which is located near the C-terminal region of the protein monitors the effect of conformational dynamics on the ET rate from dansyl to DNA. It is also known that upon complexation with operator DNA, the N-terminal domain of the protein becomes frozen, while the C-terminal domain shows flexibility (12) of different degrees. In this regard, electron transfer dynamics from the dansyl to operator DNA has been studied. In principle, dansyl can also act as an electron donor or hole acceptor, retrieving the native state of guanine from its radical cation as the oxidation potential of N-ethyl dansylamide (0.94 V), a derivative of dansyl, is lower than the oxidation potential of guanine (58). The electron transfer dynamics of dansyl in the protein upon complexation with  $O_{R1}$  and  $O_{R2}$  DNA is evident from the faster fluorescence transients depicted in Figure 20(B). ET rate is found to be similar for both repressor- $O_{R1}/O_{R2}$  DNA complex ( $1.2 \times 10^8/s$  and  $1.0 \times 10^8/s$  for repressor- $O_{R1}/O_{R2}$  DNA complex, respectively). This may be because the different conformations of the dansyl chromophore as a consequence of dynamical flexibility of the protein have similar ET efficiency to the DNA.

## Conclusion

The studies under review provide substantial insight into the structural and dynamical aspects in protein-DNA interaction, which explore the fundamentals of biomolecular recognition in such interactions.

Structural studies on the protein-DNA complex (both DNA and protein are from calf thymus) reveal a compact-globular type, in contrast to the hollow-toroid type of the interspecies complex (DNA and protein are from salmon sperm and calf thymus). In the case of genomic DNA molecules, solvation studies depict an insignificant change in the local environments of DNA molecules upon complexation with histone 1. Fluorescence anisotropy studies on the minor groove binder H33258 in DNA and in the complex clearly rule out the possibility of detachment of any minor groove-binding drug with the DNA in the complex. In contrast to the minor groove-binding, a significant perturbation in the intercalative interaction of EtBr with various DNA molecules including synthetic oligonucleotide upon complexation with H1 clearly

demonstrate that the base-stacking is heavily perturbed in the DNA-H1 complexes. Perturbation of base-stacking as revealed by intercalation of EtBr probably follows the consequence of the change in the conformation of the DNA in the complex. These observations are important to understand the binding of drug molecules in the linker DNA of nucleosome core particles. The other femtosecond-resolved dynamical studies on histone protein interaction reveals that the highly rigid H1-DNA complex and the strong binding in the recognition of DNA by the protein H1 are perhaps key features in the sealing of the linker DNA during the nucleosome formation. These studies attempt to link structural and dynamical features for insight into the biological function of nucleosome formation and chromatin condensation.

While, exploring the specific protein-DNA interaction at  $\lambda$ -repressor-operator sites interaction, particularly  $O_{R1}$  and  $O_{R2}$ , it was observed that the interfacial water dynamics is minimally perturbed upon interaction with DNA, suggesting the labile interface in the protein-DNA complex. Fluorescence anisotropy study reveals enhanced flexibility of the C-terminal domain of the repressor at fast timescales after complex formation with  $O_{R1}$ . In contrast,  $O_{R2}$  bound repressor shows no significant enhancement of protein dynamics at these timescales. These differences are shown to be important for correct protein-protein interactions. DNA induced allostery in protein structure and dynamics is found to be an integral part of such interaction. Also, the role of such differential conformation has profound effect in the PET process. Altered protein dynamics upon specific DNA sequence recognition may play important roles in assembly of regulatory proteins at the correct positions.

**Acknowledgments:** SB and SC thank CSIR (India) for the research fellowships. We thank DST (India) for financial grants (SB/S1/PC-011/2013 and DST/TM/SERI/2k11/103). We are extremely grateful to Prof. Siddhartha Roy (Indian Institute of Chemical Biology, Kolkata) for allowing us to work in his laboratory for lambda repressor isolation and purification. We would also like to thank our colleagues and collaborators whose contributions over the years, acknowledged in the references, have been priceless in the successful evolution of work in this area. In particular, we thank Prof. Ahmed H. Zewail, Prof. Dongping Zhong, Dr. Rupa Sarkar and Dr. Abhishek Mazumder.

Received December 4, 2013; accepted January 15, 2014

## References

1. Matysiak S, Debenedetti PG, Rossky PJ. Role of hydrophobic hydration in protein stability: a 3D water-explicit protein model exhibiting cold and heat denaturation. *J Phys Chem B* 2012; 116: 8095–104.
2. Somani S, Chng CP, Verma CS. Hydration of a hydrophobic cavity and its functional role: a simulation study of human interleukin-1 $\beta$ . *Proteins* 2007; 67: 868–85.
3. Levy Y, Onuchic JN. [Water mediation in protein folding and molecular recognition](#). *Annu Rev Biophys Biomol Struct* 2006; 35: 389–415.
4. Giovambattista N, Lopez CF, Rossky PJ, Debenedetti PG. [Hydrophobicity of protein surfaces: separating geometry from chemistry](#). *Proc Natl Acad Sci USA* 2008; 105: 2274–9.
5. Rydberg P, Rod TH, Olsen L, Ryde U. Dynamics of water molecules in the active-site cavity of human cytochromes P450. *J Phys Chem B* 2007; 111: 5445–57.
6. Orphanides G, Reinberg D. A unified theory of gene expression. *Cell* 2002; 108: 439–51.
7. Kalodimos CG, Biris N, Bonvin AMJJ, Levandoski MM, Guennuegues M, Boelens R, Kaptein R. Structure and flexibility adaptation in nonspecific and specific protein-DNA complexes. *Science* 2004; 305: 386–9.
8. Muller C, Calsou P, Frit P, Salles B. Regulation of the DNA-dependent protein kinase (DNA-PK) activity in eukaryotic cells. *Biochimie* 1999; 81: 117–25.
9. Koop AH, Staprans SI, Bourgeois S. Specific binding of the cAMP receptor protein of *Escherichia coli* to the lactose operon promoter. *Biochimie* 1985; 67: 161–75.
10. Rohs R, Jin XS, West SM, Joshi R, Honig B, Mann RS. [Origins of specificity in protein-DNA recognition](#). *Annu Rev Biochem* 2010; 79: 233–69.
11. Roy S. Protein-DNA and protein-protein interactions in  $\lambda$ -repressor/operator system: a review. *Curr Sci India* 1996; 71: 100–6.
12. Saha R, Banik U, Bandyopadhyay S, Mandal NC, Bhattacharyya B, Roy S. An operator-induced conformational change in the C-terminal domain of the  $\lambda$  repressor. *J Biol Chem* 1992; 267: 5862–7.
13. Deb S, Bandyopadhyay S, Roy S. Spectroscopic study of Y210C  $\lambda$ -repressor: implications for cooperative interaction. *Protein Eng* 1998; 11: 481–7.
14. Ptashne M. *A genetic switch: phage  $\lambda$  and higher organisms*. Boston, USA: Cell Press, 1992.
15. Jana NK, Deb S, Bhattacharyya B, Mandal NC, Roy S. [A study of energetics of cooperative interaction using a mutant  \$\lambda\$ -repressor](#). *Protein Eng* 2000; 13: 629–33.
16. Jordan SR, Pabo CO. Structure of the  $\lambda$  complex at 2.5 Å resolution: details of the repressor-operator interactions. *Science* 1988; 242: 893–9.
17. Zhong D, Pal SK, Zewail AH. [Femtosecond studies of protein-DNA binding and dynamics: histone I](#). *ChemPhysChem* 2001; 2: 219–27.
18. Tzeng SR, Kalodimos CG. Protein activity regulation by conformational entropy. *Nature* 2012; 488: 236–40.
19. Tzeng SR, Kalodimos CG. Dynamic activation of an allosteric regulatory protein. *Nature* 2009; 462: 368–72.
20. Popovych N, Tzeng SR, Tonelli M, Ebricht RH, Kalodimos CG. [Structural basis for cAMP-mediated allosteric control of the catabolite activator protein](#). *Proc Natl Acad Sci USA* 2009; 106: 6927–32.
21. Yu B, Blaber M, Gronenborn AM, Clore GM, Caspar DLD. Disordered water within a hydrophobic protein cavity visualized by x-ray crystallography. *Proc Natl Acad Sci USA* 1999; 96: 103–8.
22. Sarkar, R, Pal SK. Interaction of Hoechst 33258 and ethidium with histone1-DNA condensates. *Biomacromolecules* 2007; 8: 3332–9.
23. Pabo CO, Sauer RT, Sturtevant JM, Ptashne M. [The  \$\lambda\$  repressor contains two domains](#). *Proc Natl Acad Sci USA* 1979; 76: 1608–12.
24. Hochschild A, Ptashne M. [Cooperative binding of  \$\lambda\$  repressors to sites separated by integral turns of the DNA helix](#). *Cell* 1986; 44: 681–7.
25. Senear DF, Brenowitz M, Shea MA, Ackers GK. [Energetics of cooperative protein-DNA interactions: comparison between quantitative deoxyribonuclease footprint titration and filter binding](#). *Biochemistry* 1986; 25: 7344–54.
26. Benson N, Adams C, Youderian P. [Genetic selection for mutations that impair the co-operative binding of  \$\lambda\$  repressor](#). *Mol Microbiol* 1994; 11: 567–79.
27. Mondol T, Batabyal S, Pal SK. [Ultrafast electron transfer in the recognition of different DNA sequences by a DNA-binding protein with different dynamical conformations](#). *J Biomol Struct Dyn* 2012; 30: 362–70.
28. Mondol T, Batabyal S, Mazumder A, Roy, S, Pal SK. Recognition of different DNA sequences by a DNA-binding protein alters protein dynamics differentially. *FEBS Lett* 2012; 586: 258–62.
29. Batabyal S, Rakshit S, Kar S, Pal SK. An improved microfluidics approach for monitoring real-time interaction profiles of ultrafast molecular recognition. *Rev Sci Instrum* 2012; 83: 043113–6.
30. Lakowicz JR. *Principles of fluorescence spectroscopy*. New York, USA: Kluwer Academic/Plenum, 2006.
31. Batabyal S, Mondol T, Choudhury S, Mazumder A, Pal SK. Ultrafast interfacial solvation dynamics in specific protein DNA recognition. *Biochimie* 2013; 95: 2168–76.
32. Banerjee D, Pal SK. Ultrafast charge transfer and solvation of DNA minor groove binder: Hoechst 33258 in restricted environments. *Chem Phys Lett* 2006; 432: 257–62.
33. Sarkar R, Ghosh M, Shaw AK, Pal SK. Ultrafast surface solvation dynamics and functionality of an enzyme  $\alpha$ -chymotrypsin upon interfacial binding to a cationic micelle. *J Photochem Photobiol B Biol* 2005; 79: 67–78.
34. Pal SK, Zhao LA, Zewail AH. [Water at DNA surfaces: Ultrafast dynamics in minor groove recognition](#). *Proc Natl Acad Sci USA* 2003; 100: 8113–8.
35. Fee RS, Maroncelli M. Estimating the time-zero spectrum in time-resolved emission measurements of solvation dynamics. *Chem Phys* 1994; 183: 235–47.
36. Brauns EB, Madaras ML, Coleman RS, Murphy CJ, Berg MA. Measurement of local DNA reorganization on the picosecond and nanosecond time scales. *J Am Chem Soc* 1999; 121: 11644–9.
37. Parkinson JA, Ebrahimi SE, Mckie JH, Douglas KT. Molecular design of DNA-directed ligands with specific interactions –

- solution NMR-studies of the interaction of a M-hydroxy analog of Hoechst-33258 with D(CGCGAATTCGCG)(2). *Biochemistry* 1994; 33: 8442–52.
38. Sheffield VC, Cox DR, Lerman LS, Myers RM. Attachment of a 40-base-pair G + C-rich sequence (GC-clamp) to genomic DNA fragments by the polymerase chain reaction results in improved detection of single-base changes. *Proc Natl Acad Sci USA* 1989; 86: 232–6.
  39. Chitre AV, Korgaonkar KS. Binding of ethidium bromide and quinacrine hydrochloride to nucleic acids and reconstituted nucleohistones. *Biochem J* 1979; 179: 213–9.
  40. Sarkar R, Pal SK. Ligand–DNA interaction in a nanocage of reverse micelle. *Biopolymers* 2006; 83: 675–86.
  41. Homoelle BJ, Edington MD, Diffey WM, Beck WF. [Stimulated photon-echo and transient-grating studies of protein-matrix solvation dynamics and interexciton-state radiationless decay in alpha phycocyanin and allophycocyanin.](#) *J Phys Chem B* 1998; 102: 3044–52.
  42. Jordanides XJ, Lang MJ, Song XY, Fleming GR. Solvation dynamics in protein environments studied by photon echo spectroscopy. *J Phys Chem B* 1999; 103: 7995–8005.
  43. Lawrence JJ, Berne L, Ouvrier-Buffet JL, Piette LH. Spin-label study of histone H1-DNA interaction. Comparative properties of the central part of the molecule and the N and C-amino tails. *Eur J Biochem* 1980; 107: 263–9.
  44. Wang HF, Borguet E, Eisinger KB. [Polarity of liquid interfaces by second harmonic generation spectroscopy.](#) *J Phys Chem A* 1997; 101: 713–8.
  45. Banik U, Saha R, Mandal NC, Bhattacharyya B, Roy S. Multiphasic denaturation of the  $\lambda$  repressor by urea and its implications for the repressor structure. *Eur J Biochem* 1992; 206: 15–21.
  46. Banik U, Mandal NC, Bhattacharyya B, Roy S. A fluorescence anisotropy study of tetramer-dimer equilibrium of  $\lambda$ -repressor and its implication for function. *J Biol Chem* 1993; 268: 3938–43.
  47. Zhong D, Pal SK, Wan C, Zewail AH. Femtosecond dynamics of a drug-protein complex: daunomycin with Apo riboflavin-binding protein. *Proc Natl Acad Sci USA* 2001; 98: 11873–8.
  48. Köddermann T, Ludwig R, Paschek D. On the validity of Stokes–Einstein and Stokes–Einstein–Debye relations in ionic liquids and ionic-liquid mixtures. *ChemPhysChem* 2008; 9: 1851–8.
  49. Sarkar R, Ghosh M, Pal SK. Ultrafast relaxation dynamics of a biologically relevant probe dansyl at the micellar surface. *J Photochem Photobiol B* 2005; 78: 93–8.
  50. Mondol T, Batabyal S, Pal SK. Interaction of an antituberculosis drug with nano-sized cationic micelle: Förster resonance energy transfer from dansyl to rifampicin in the microenvironment. *Photochem Photobiol* 2012; 88: 328–35.
  51. Tachiya M. Application of a generating function to reaction kinetics in micelles. Kinetics of quenching of luminescent probes in micelles. *Chem Phys Lett* 1975; 33: 289–92.
  52. Banerjee S, Tachiya M, Pal SK. Caffeine-mediated detachment of mutagenic ethidium from various nanoscopic micelles: an ultrafast Förster resonance energy transfer study. *J Phys Chem B* 2012; 116: 7841–8.
  53. Sadhu S, Tachiya M, Patra A. A stochastic model for energy transfer from CdS quantum dots/rods (donors) to Nile red dye (acceptors). *J Phys Chem C* 2009; 113: 19488–92.
  54. Banerjee D, Pal SK. Direct observation of essential DNA dynamics: melting and reformation of the DNA minor groove. *J Phys Chem B* 2007; 111: 10833–8.
  55. Milligan JR, Aguilera JA, Ly A, Tran NQ, Hoang O, Ward JF. [Repair of oxidative DNA damage by amino acids.](#) *Nucleic Acids Res* 2003; 31: 6258–63.
  56. Robel I, Kuno M, Kamat PV. Size-dependent electron injection from excited CdSe quantum dots into TiO<sub>2</sub> nanoparticles. *J Am Chem Soc* 2007; 129: 4136–7.
  57. Isied SS, Ogawa MY, Wishart JF. Peptide-mediated intramolecular electron transfer: long-range distance dependence. *Chem Rev* 1992; 92: 381–94.
  58. Guy J, Caron K, Dufresne S, Michnick SW, Skene WG, Keillor JW. Convergent preparation and photophysical characterization of dimaleimide dansyl fluorogens: elucidation of the maleimide fluorescence quenching mechanism. *J Am Chem Soc* 2007; 129: 11969–77.